POLITECNICO DI TORINO

Collegio di Ingegneria Chimica e dei Materiali

Corso di Laurea Magistrale
in Ingegneria Chimica e dei Processi Sostenibili

Tesi di Laurea Magistrale

Kinetic modelling applied to selective hydrogenation of polyunsaturated hydrocarbons on innovative alveolar monoliths

Relatore

Prof.ssa Specchia Stefania

Candidato

Marchisio Elia

Marzo 2019

To Enrico, Fabrizio, Licia, Amina, Sofia, Leonor, Ana, Charles, Rita, Bruno, Mariana, Kike, Jano, and Simone

Index

Prefazione alla Tesi di Laurea Magistrale IV

1 Introduction 1

2 Motivations and objectives 3

3 State of the art 4

3.1 Refineries 4
3.2 Cracking 4
3.3 Selective hydrogenation 6
3.4 Catalysis 7
3.5 Reactors and operating conditions 8
3.6 Innovative monolithic materials 11
3.7 Alveolar monolith synthesis via sol-gel process 11

4 Model 14

4.1 Assumptions 14
4.2 Kinetic equations 15
4.3 Reaction Mechanism 16
4.4 Mass balance equations 17
4.5 Parameters derivation 21

5 Computational algorithm 23

5.1 BVP solution 24
5.2 DAE solution 24
5.3 Pressure drop computation 24

6 Results 27

6.1 Catalytic wall profiles 27
6.1.1 C_4 hydrogenation wall profile 27
6.1.2 C_3 hydrogenation wall profile 29
6.1.3 C_2 hydrogenation wall profile 30
6.2 Overall reactor profiles 32
6.2.1 Simulations 32
6.2.2 C_4 hydrogenation reactor profile 33
6.2.3 C_3 hydrogenation reactor profile 37
6.2.4 C_2 hydrogenation reactor profile 40
6.3 Comparisons 42
6.4 Pressure drops 45
6.5 Summary 46
6.6 Troubleshooting 48

7 Conclusions 51

Reference list 58

8 Acknowledgements 60

Prefazione alla Tesi di Laurea Magistrale

1 Introduzione

L'idrogenazione è un processo molto comune nelle raffinerie. Negli ultimi decenni, la richiesta del mercato di prodotti a base di petrolio è cambiata, favorendo carburanti più leggeri ed olefine (come l'etilene). Ciò ha infine costretto le raffinerie ad implementare più unità di idrogenazione.
L'idrogenazione selettiva, in particolare, è un processo adottato al fine di idrogenare le insaturazioni nei tagli petroliferi, ma preservando prodotti di alto valore aggiunto come le olefine.
In dettaglio, questo tipo di idrogenazione è adottato dopo l'operazione di *fluid catalitic cracking* ed in particolare dopo lo *steam cracking*, con lo scopo di trasformare prodotti poli-insaturi in mono-insaturi, basi per la produzione di polimeri ed altri prodotti petrolchimici.
I tagli di principale interesse in questa operazione, trattasi di C_2, C_3, C_4, sono stati considerati in questo lavoro.
Dal momento che il mercato richiede un'elevatissima purezza per le basi mono-insature, l'uso di sistemi catalitici *ad hoc* è necessario per garantire la selettività dell'idrogenazione.
Per l'operazione si utilizzano sistemi a letto fisso, nel quale il catalizzatore è adagiato in forma di pellets di varie forme possibili. I pellets sono di norma realizzati in g-allumina, sulla quale come principio attivo è disperso del palladio, questo rappresenta la soluzione più adottata per garantire attività e selettività.
Fissate le condizioni operative, la performance del sistema catalitico, a parità di principio attivo usato, dipenderà dalla morfologia (*texture properties*) del catalizzatore.
Tra queste proprietà troviamo area specifica, lunghezza di diffusione nel solido, porosità e sue caratteristiche.
Per un miglioramento della morfologia, supporti monolitici alveolari possono essere considerati come soluzione alternativa ai pellets.

2 Scopo ed obbiettivi

Lo scopo del lavoro di tesi è stato quello di studiare un approccio innovativo all'idrogenazione selettiva, consistente nell'adozione di supporti monolitici alveolari con porosità gerarchica, in sostituzione ai pellets, come supporto catalitico.
Questi sistemi non sono al momento adottati negli impianti industriali e presenterebbero potenziali vantaggi, la struttura dei monoliti alveolari garantisce infatti elevata area superficiale, minore lunghezza diffusiva e minore perdita di carico grazie alla maggiore porosità.
Questo lavoro è stato realizzato in previsione della futura sintesi di tali supporti monolitici per la sperimentazione in laboratorio o su impianto pilota. L'obbiettivo è stato dunque quello di realizzare un modello cinetico per descrivere il sistema. Per cominciare sono state fatte le necessarie ipotesi semplificative in modo da rendere possibile la creazione e soluzione del modello nel tempo disponibile. Successivamente sono state scritte le equazioni di bilancio e le condizioni al contorno, infine il sistema è stato risolto mediante un algoritmo computazionale, quest'ultimo è stato programmato sul software *Matlab*.
Una volta raggiunte soluzioni accettabili, ossia tali da validare l'affidabilità di equazioni, algoritmo e metodo risolutivo, analisi di sensitività sono state effettuate per determinare le *texture properties* che garantissero le migliori prestazioni del monolita. In conclusione, un tentativo di confronto con i *pellets* è stato proposto cercando di adattare l'algoritmo alla risoluzione del sistema convenzionale. Tutte le analisi di sensitività sono state condotte sul parametro di principale interesse in questa idrogenazione, la *selettività*, considerando quindi pari quantità di principio attivo, un'ulteriore serie di analisi è stata effettuata per valutare e confrontare anche le perdite di carico.
A scopo di chiarimento, si può ora specificare che i potenziali vantaggi di cui si è accennato in precedenza, portati dal supporto innovativo, consistono dunque in un risparmio energetico (minori perdite di carico) e soprattutto in un risparmio di principio attivo (palladio), principale indice di costo del catalizzatore, così da giustificare l'adozione del monolita.
Per concludere, sono elencate in seguito le fasi con cui si sono scanditi i cinque mesi di lavoro:

stesura ipotesi, stesura delle equazioni, programmazione, analisi di sensitività; E'opportuno riportare che gran parte del tempo è stato dedicato alla fase di programmazione (stesura dello *script*, algoritmi considerati e *debugging*) la quale costituisce infine il corpo del lavoro di tesi, ma di cui solo l'algoritmo finale è presentato.

3 Idrogenazione selettiva

Come già accennato, questa operazione si ha soprattutto dopo il processo di *steam cracking* e riguarda in particolare i tagli C_2, C_3, C_4 come riportato in *figure 4* nell'elaborato.
Le specifiche di purezza richieste sono qui riportate in *table 1*, l'impurità è costituita dal composto poli-insaturo mentre il prodotto di interesse è quello mono-insaturo.
Anticipando le semplificazioni del modello cinetico, possiamo dividere i composti di ogni taglio in tre gruppi (A, B, C) rappresentanti nell'ordine i composti poli-insaturi, monoinsaturi e saturi presenti nel taglio. Detto ciò, in *table 2* è possibile osservare la composizione tipica dei tagli alimentati, qui riportata insieme alla cinetica in *figure 13* per maggiore chiarezza.
Risulta chiaro che la selettività ha lo scopo di massimizzare il composto B della reazione consecutiva.

Feed	**Impurity (A)**	**Product of interest (B)**	**Specification (mass ppm)**
Cut C_2	Acetylene	Ethylene	<5
Cut C_3	Propyne, propadiene, methylacetylene	Propylene	<10
Cut C_4	1,3 Butadiene	Butenes	<10

Table 1: Selective hydrogenation specifications for production of intermediaries for petrochemistry (figure from (Thomazeau and Boyer, 2011) with modifications)

$$A \xrightarrow[r_1]{H_2} B \xrightarrow[r_2]{H_2} C$$

Figure 1: Reaction scheme for hydrogenation of polyunsaturated compounds

Molar fraction			
Feed	**A**	**B**	**C**
Cut C_2	0.014	0.687	0.294
Cut C_3	0.045	0.915	0.050
Cut $C_4{}^*$	0.005	0.932	0.063

Table 2: Molar fractions of C_2 to C_4 cuts after cracking and separation steps; A: polyunsaturated compound, B: monounsaturated compound, C: saturated compound. *cut C_4 composition after extraction of 1,3-butadiene. (figure from (Thomazeau and Boyer, 2011) with modifications)

Considerando ora il sistema reattivo, abbiamo che il letto fisso può essere mono o multi-tubolare, operare in uno o più stadi, in fase liquida, gas o mista ed infine in condizioni adiabatiche o isoterme.
La condizione adiabatica è solitamente quella scelta poiché, essendo l'idrogenazione una reazione fortemente esotermica, un agevole controllo dei profili di temperatura è fattibile solo in un sistema multi-tubolare, i sistemi a più stadi con raffreddamento intermedio possono essere considerati un ibrido tra le due condizioni.
Le condizioni operative dipendono dal taglio, per C_2, C_3, C_4 sono normalmente nel range 10-25 bar, si usano pressioni inferiori se si opera in fase gas (nel caso di C_2 questa è l'unica soluzione) e la temperatura è compresa tra 20 e 100°C per favorire la reazione (poichè esotermica). Uno schema di processo di idrogenazione selettiva in ambito industriale è mostrato in *figure 6*.

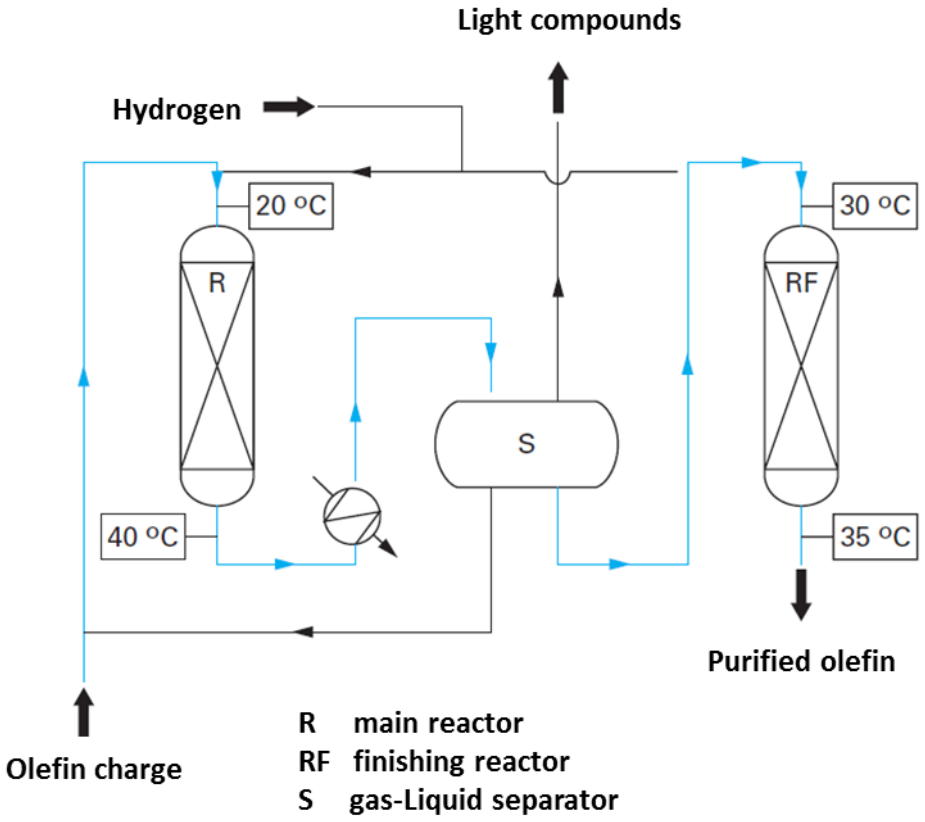

Figure 2: scheme of a selective hydrogenation process for C3 cut, configuration with two adiabatic reactors (multi-stage) with intercooling and a separation step (figure from (Thomazeau and Boyer, 2011) with modifications)

4 Supporti monolitici innovativi

I supporti monolitici sono realizzati con materiali ceramici o con metalli (o leghe metalliche) e presentano strutture caratterizzate da canali paralleli (come un nido d'ape).
Essi sono già utilizzati in ambito industriale in diversi settori quali *automotive*, ambiente (trattamento NOx) ed altri. Il loro vantaggio rispetto ai pellets consiste nelle basse perdite di carico, dovute all'elevata porosità e alla loro *open frontal area*. Con essi si limitano inoltre i fenomeni di attrito e si ha la possibilità di realizzare *layer* più sottili su cui depositare il principio attivo, così da limitare il controllo diffusivo.
Il supporto monolitico oggetto della modellizzazione ha invece caratteristiche strutturali del tutto innovative, si tratta di un monolita alveolare con porosità gerarchica, ovvero con due classi di grandezza dei pori. Nelle pareti che compongono la prima classe di pori si trovano i pori più piccoli, questi ultimi sviluppano nel solido elevate aree superficiali, la loro lunghezza è circa la metà dello spessore delle pareti (*shell walls*), queste

possono essere sottili fino a pochi *micron*, così da limitare al massimo il controllo diffusivo. La struttura gerarchica di questo supporto è rappresentata in *figure 2*.

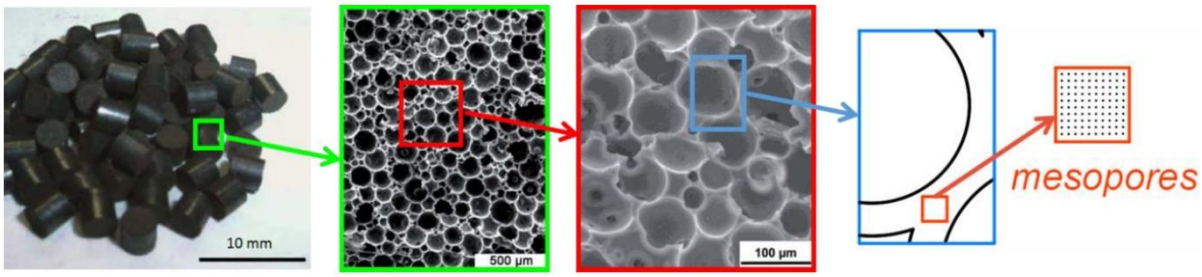

Figure 3: Pictures of monoliths (right), MEB pictures of alveolar monoliths and representation of the wall (figure from (Destribats *et al.*, 2012) with modifications)

Infine, i monoliti alveolari possono essere sintetizzati con ampio *range* di dimensione dei pori e spessore delle pareti.
I parametri usati nel modello cinetico considerano monoliti alveolari prodotti come polimeri di *HIPE* (*high internal phase emulsions)* a base di silice. Questi sono sintetizzati con processo *sol-gel* partendo dalla silice che agisce da monomero-precursore ed è soggetta a reazioni di *cross-linking* che avvengono in soluzione. Durante la sintesi si ha la formazione di un gel, la cui struttura finale è facilmente controllata dalle condizioni operative. Il monolita sintetizzato (noto come *SiPHIPE*) presenta porosità fino ad oltre 90% ed area specifica (*BET*) di 700-900 m^2/g, i macro-pori hanno diametro nel *range* 20-500 *micron* e meso-pori di 4-11 *micron* con stretta *pore size distribution*, infine lo spessore delle pareti può essere sottile fino a pochi *micron*.

5 Modello cinetico

5.1 Ipotesi

Si è scelto di modellare il sistema come un *plug flow reactor* (*figure 11* nell'elaborato), il monolita è considerato come un cilindro di volume uguale a quello del reattore. In seguito sono riportate le ipotesi principali del modello:

- Assenza di dispersione radiale
- Condizioni stazionarie
- Portata costante della fase liquida
- Sistema isotermo ed isobaro
- Alimentazione in equi-corrente dal basso verso l'alto (*up-flow*)
- Bagnatura completa della superfice catalitica
- Alimentazione all'equilibrio termodinamico liquido-gas
- Fase gas avente comportamento ideale

Come detto in precedenza, negli impianti si adottano di norma sistemi adiabatici, in questo modello il sistema è invece isotermo così che i bilanci di energia possano non essere considerati, questa assunzione è stata fondamentale per semplificare il sistema e dunque la programmazione dell'algoritmo.

5.2 Cinetica

Come mostrato in *figure 13*, lo schema di reazione è semplificato in due reazioni consecutive. Maggiore è il numero di atomi di carbonio nel reagente maggiore sarà la quantità di isomeri che possono formarsi per la specie mono-insatura (B), infatti nel caso di C_4,ad esempio, si ha che B comprende più isomeri di butene in equilibrio tra loro. La prima semplificazione riguarda dunque lo schema di reazione e consiste nel raggruppare le specie con lo stesso livello di saturazione in un solo componente.
Per quanto riguarda il meccanismo di reazione, il modello di *Langmuir-Hinshelwood-Hougen-Watson* (*LHHW*) è stato adottato come in numerosi casi in letteratura che descrivono reazioni di idrogenazione selettiva. Il modello introduce diverse semplificazioni, tuttavia, le equazioni cinetiche prodotte presentano ugualmente molti parametri poiché tengono conto di tre reazioni: adsorbimento, reazione superficiale e desorbimento della specie. Per questa ragione uno dei tre meccanismi può essere considerato controllante, da esempi di letteratura che considerano la reazione superficiale come step controllante. Le cinetiche sono state dunque espresse come in *equation 4.2.*

$$\boldsymbol{r_1 = \frac{k_1 x_A x_{H_2}}{1+K_A x_A+K_B x_B}\ ;\ r_2 = \frac{k_2 x_B x_{H_2}}{1+K_A x_A+K_B x_B}} \qquad \textbf{(4.2)}$$

5.3 Equazioni di bilancio di materia

In primo luogo, è opportuno ricordare la struttura dei monoliti alveolari (riportata in *figure 2* e *figure 9*), considerando ora un cilindro monolitico costituente il volume di reattore, abbiamo che le equazioni di bilancio possono essere divise in tre gruppi: bilancio nella parete (*shell wall*), bilancio interno di un volume infinitesimo di reattore (*micro-kinetics equations*) ed infine il bilancio tra due volumi infinitesimi adiacenti del reattore (*macro-kinetics equations*).
Riguardo il bilancio alla parete, abbiamo che si considera solo trasporto diffusivo, governato dalla legge di Fick, si hanno qui equazioni differenziali del secondo ordine con condizione ai bordi (*BVP*) (*equation 4.3*). Va specificato che il profilo che si forma nella parete è simmetrico, infatti i micro-pori nelle pareti si estendono, partendo dalla superfice, idealmente fino a metà della parete (L è il semi-spessore della parete), come rappresentato in *figure13*.
La condizione imposta per il centro della parete (fondo del poro) è di avere profilo piatto di concentrazione (dunque derivata nulla).

$$\boldsymbol{D_{e,i} C \frac{\partial^2 x_i}{\partial y^2} = \rho_w r_i} \qquad \begin{cases} \boldsymbol{x_i(y = L) = x_{iS}} \\ \boldsymbol{\frac{dx_i}{dy}(y = 0) = 0} \end{cases} \qquad \textbf{(4.3)}$$

$$i = A, B, C, H_2$$

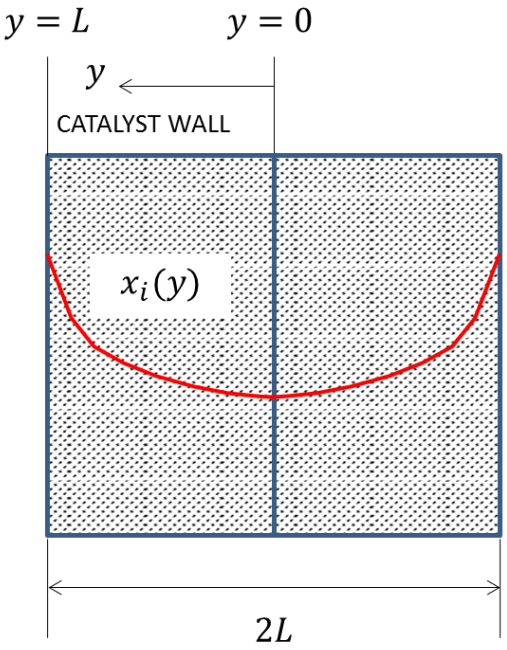

Figure 13: Graphic representation of molar fraction profile inside the wall

Solo dopo aver risolto il bilancio nella parete è possibile risolvere quello del volume infinitesimo di reattore, infatti come si vede nell'algoritmo computazionale, in *figure 16*, il *BVP* è risolto iterativamente poiché non si conosce la concentrazione delle specie alla parete. Nota questa concentrazione è possibile risolvere i bilanci micro-cinetici ricavando così tutte le concentrazioni nel volume infinitesimo, dunque è poi possibile risolvere le equazioni macro-cinetiche per aggiornare le concentrazioni e la portata di gas nel nuovo volume. Le equazioni sono riportate qui in seguito (*equation 4.4,4.5,4.6,4.7*) e rappresentate graficamente in *figure 15*, queste costituiscono un sistema di equazioni differenziali e algebriche (*DEA*).

Macro-kinetics equations (8 equations):

$$(1)\ \boldsymbol{GAS:}\quad \boldsymbol{C_{iG}\frac{d\dot{V}_G}{dz}+\dot{V}_G\frac{dC_{iG}}{dz}=-J_i^{GL}aS} \tag{4.4}$$

$$(2)\ \boldsymbol{LIQ}:\quad \boldsymbol{\dot{V}_L\frac{dC_{iL}}{dz}=J_i^{GL}aS-J_i^{LS}aS} \tag{4.5}$$

Micro-kinetics equations (8 equations):

$$(3)\ \boldsymbol{J_i^{GL}aS=k_{iL}a_LS\left(\frac{C_{iG}}{H_i}-C_{iL}\right)} \tag{4.6}$$

$$(4)\ \boldsymbol{J_i^{LS}aS=k_{iS}a_SS(C_{iL}-C_{iS})=\rho_w\eta R_{iS}(1-\varepsilon_B)} \tag{4.7}$$

Where: $i = A, B, C, H_2$

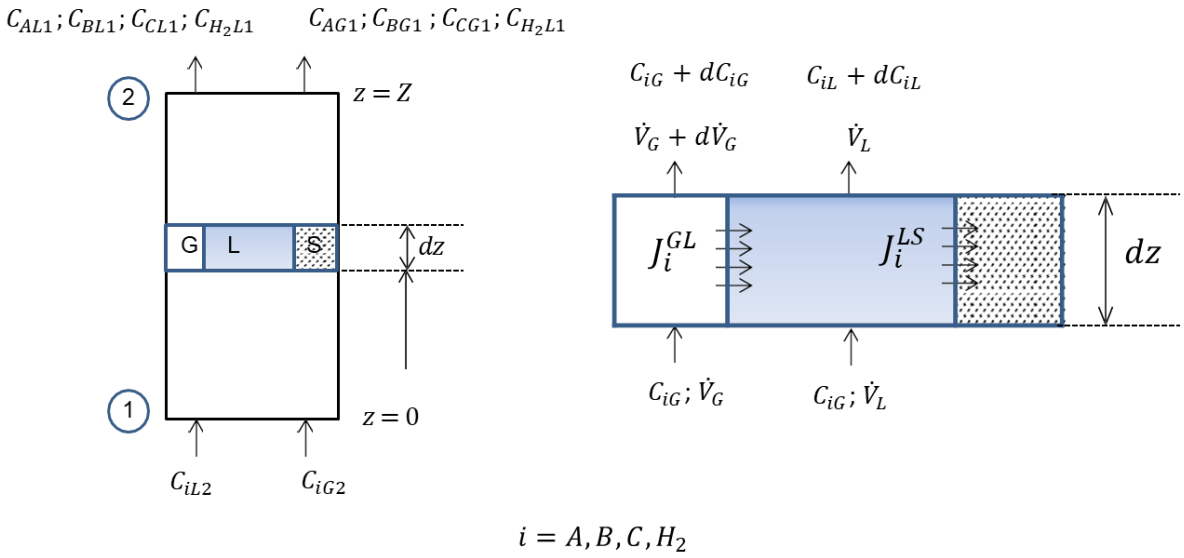

Figure 14: Three-phase reactor graphic representation, overall reactor (left), infinitesimal volume (right)

I parametri di trasferimento di massa nei bilanci sono ricavati in letteratura, molte correlazioni sono diverse per i monoliti rispetto ai pellets, per quanto riguarda questi ultimi si è scelto di considerare sfere di pochi millimetri di diametro con strato esterno in g-allumina (scelta comune in industria). Per esprimere l'area superficiale del reattore (non micro-porosa) dei supporti, si sono adottate correlazioni geometriche. Mentre per letti fissi con pellets si può adottare una semplice correlazione ampiamente usata in letteratura (*table I*). Per quanto riguarda il supporto innovativo, la semplice espressione matematica è stata proposta ex novo (*table I*). Essa tiene conto del diametro dei macro-pori (d_M), dello spessore delle pareti (2L) e di diametro e numero delle connessioni tra macro-pori (d_{conn}, N_{conn}). I parametri relativi alle connessioni sono fissati ad un valore costante, la correlazione esprime in modo semplificato l'area specifica senza considerare le irregolarità degli alveoli, come si può dedurre in *figure 1* nell'elaborato.

Alveolar monolith:	*Spherical pellets:*
$a_{iS} = \frac{{d_M}^2\pi - [{d_{conn}}^2 N_{conn}\pi/4]}{[(d_M + 2L)^3 - {d_M}^3]\pi/6}$	$a_{iS} = \frac{6}{d_{sp}}(1 - \varepsilon_B)$
$\varepsilon_{Bm} = \frac{{d_M}^3\pi/6}{[(d_M + 2L)^3\pi/6] - L{d_{conn}}^2 N_{conn}\pi/4}$	$\varepsilon_B = 1 - \pi/6$

Table I: geometric correlations adopted in the model

6 Algoritmo computazionale

L'algoritmo è stato scritto su *Matlab,* la ricerca della logica risolutiva, l'implementazione dei *tools* per risolvere le equazioni differenziali e le fasi di *debugging* hanno costituito la gran parte del lavoro di tesi. La logica di soluzione è schematizzata in *figure 16*, abbiamo che, una volta fissate le condizioni operative, un primo ciclo di calcolo è dedicato a determinare le concentrazioni alla parete, queste sono inizialmente ipotizzate per permettere la risoluzione del *BVP*, queste sono poi ricalcolate iterativamente tramite bilancio (4) (*equation 4.7*). Il ciclo si ripete finché le concentrazioni superficiali arrivano a convergenza (lo scarto con il valore precedente è divenuto trascurabile), a questo punto si entra nel secondo ciclo (il quale non è iterativo) dove i valori di coordinata assiale, concentrazioni e portata gassosa sono variati, tramite i bilanci macro-cinetici (*equation 4.5*), per il volume infinitesimo di reattore successivo. L'algoritmo si ripete fino al termine

della lunghezza del reattore. Si anticipa che le dimensioni del sistema sono quelle di un reattore di laboratorio e sono state prese in letteratura considerando uno studio di idrogenazione selettiva su pellets.
L'algoritmo usato deve risolvere due diversi sistemi di equazioni, per quanto riguarda il *BVP* abbiamo che la sua risoluzione è stata possibile tramite l'ausilio di una *routine* di calcolo già implementata in *Matlab*. Considerando invece i bilanci di *equation 4.4,4.5,4.6,4.7* abbiamo dei sistemi di *DAE,* per questi sistemi nessuna *routine* di calcolo è stata utilizzata, le equazioni sono state scritte in maniera esplicita per calcolare il termine differenziale. Notare che il fattore di efficienza $\boldsymbol{\eta}$ presente nel bilancio (4) è calcolato, di volta in volta, dopo la soluzione del *BVP*. La velocità media di reazione, necessaria per il calcolo di $\boldsymbol{\eta}$, è ottenuta dopo averla calcolata in molteplici punti all'interno della parete.
Passando ora al calcolo delle perdite di carico, queste sono state calcolate in uno *script* separato, esterno all'algoritmo. Lo scopo del calcolo è di trovare la morfologia del monolita che garantisca minori perdite ed infine di confrontarlo con i pellets. Le correlazioni utilizzabili per quanto riguarda i pellets sferici sono facilmente ottenibili in letteratura, invece per il caso dei monoliti alveolari, una correlazione di letteratura ricavata per schiume solide è stata adottata per simulare il supporto, il quale non è oggi ampiamente studiato in letteratura. E' fondamentale ricordare che i sistemi bi-fasici non utilizzano la stessa correlazione dei mono-fasici, nei primi infatti l'attrito tra le due fasi influenza la caduta di pressione rendendo necessarie correlazioni più complesse.
Nel lavoro di tesi, sono stati studiati tre tagli di alimentazione, mentre per C_4, C_3 abbiamo un flusso bi-fase, per quanto riguarda C_2 si ha invece la sola fase gas.

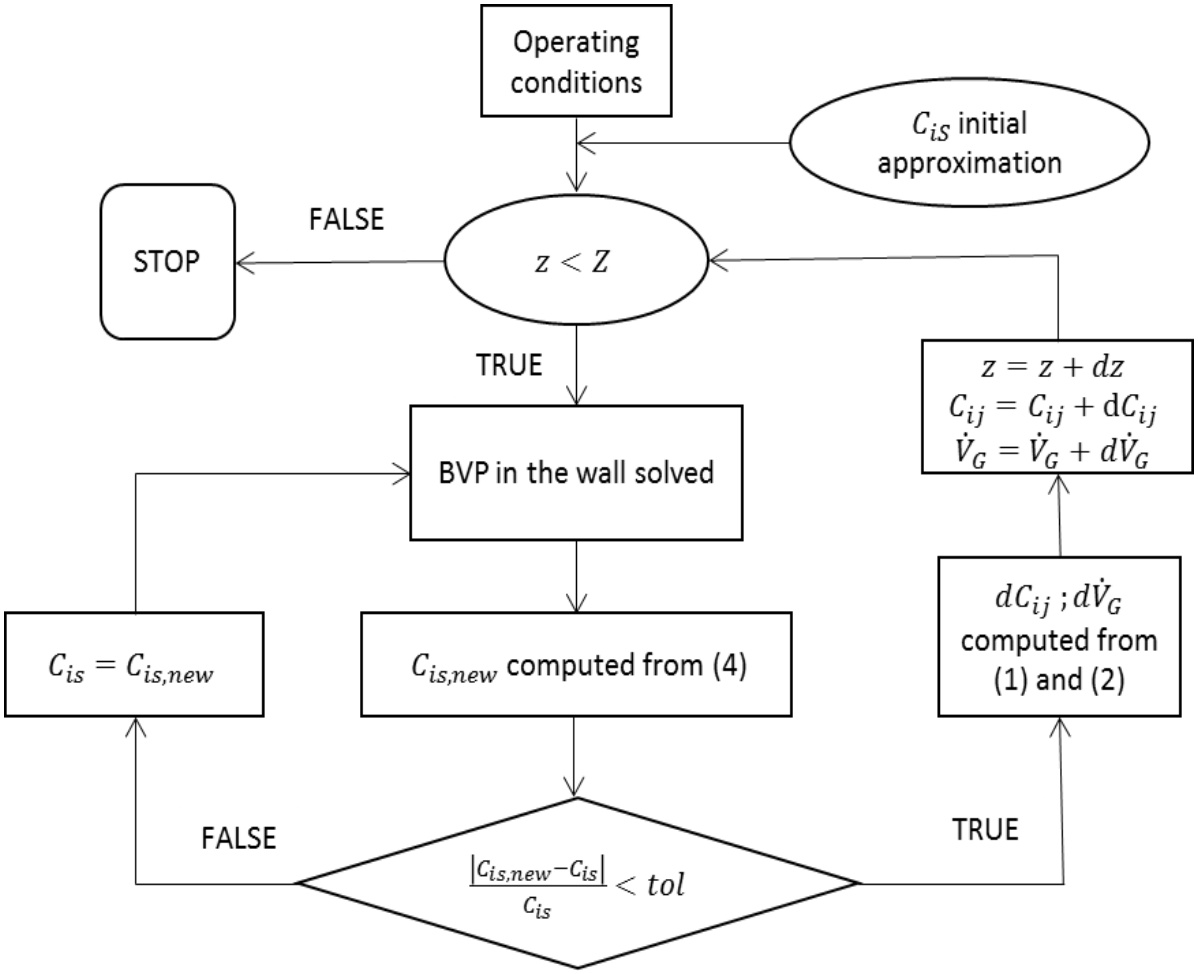

Figure 16: Schematic representation of the calculation algorithm coded on *MATLAB*

7 Risultati

7.1 Bilanci nella parete

Una prima analisi è stata condotta risolvendo solamente il bilancio nella parete *BVP,* questo per testare il funzionamento dello *script* e verificare l'effetto dello spessore della parete sui profili di concentrazione. Diversi valori del semi-spessore (L) della parete sono stati simulati per ciascun taglio.
Come già accennato la condizione imposta per il fondo dei meso-pori è di avere profilo piatto di concentrazione, in questo modo, imponendo un valore per la concentrazione all'ingresso (superfice della parete) il bilancio può essere risolto.
Con i valori di *input*, riportati in *table 7* nell'elaborato, sono stati ottenuti i profili di concentrazione. Abbiamo che il semi-spessore della parete rappresenta la lunghezza di diffusione, infatti in pareti più sottili il profilo ha maggiore tendenza ad essere piatto (*figure 17,19,20* nell'elaborato). Si riscontra anche che il taglio C_2 risulta meno sensibile allo spessore della parete (*figure 20*) in virtù della maggiore diffusività (circa due ordini di grandezza superiore rispetto a C_3, C_4) dal momento che a differenza degli altri due componenti ci troviamo in fase gas.
In conclusione, abbiamo dimostrato che pareti più sottili consentono di limitare l'impatto della diffusione, ed in maniera più marcata per i tagli C_3, C_4.

7.2 Profili di reazione nel reattore

L'obbiettivo è di raggiungere la conversione richiesta, ovvero ridurre il composto poli-insaturo A a circa 10 ppm (*table 1*) avendo la selettività finale massima possibile. In sintesi, si sono effettuate diverse analisi di sensitività, considerando due possibili alimentazioni, come nella tabella sotto riportata (*table II*). Si ricorda che i parametri analizzati (d_M, L) corrispondono al diametro dei macro-pori ed allo spessore delle pareti come riportato in *figure 10*.

Serie	Parameter	**List of analysis**				
			FEED 1		**FEED 2**	
1	Selectivity	Cut C_4	Sensitivity on d_M	Sensitivity on L	Sensitivity on d_M	Sensitivity on L
2	Selectivity	Cut C_3	Sensitivity on d_M	Sensitivity on L	Sensitivity on d_M	Sensitivity on L
3	Selectivity	Cut C_2			Sensitivity on d_M	Sensitivity on L
4	Selectivity	Cut C_4	Comparison with pellets		Comparison with pellets	
5	Selectivity	Cut C_2			Comparison with pellets	
6	Pressure drop	Cut C_4	Comparison with pellets			
7	Pressure drop	Cut C_3	Comparison with pellets			
8	Pressure drop	Cut C_2	Comparison with pellets			

Table II: summary of undertaken simulations

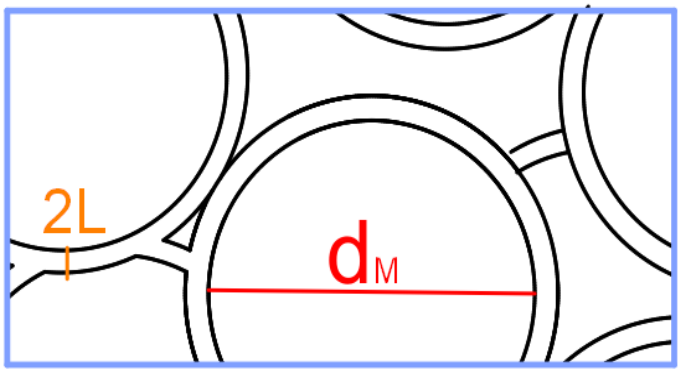

Figure 9: simplified texture of an alveolar monolith synthetized as polyHIPE

I risultati principali sono di seguito riportati secondo il numero della serie, si noti che non in tutte le simulazioni la concentrazione del componente poli-insatura A si è ridotta sotto 10 *mass ppm* come da specifiche, dunque il confronto di selettività è stato effettuato a concentrazione maggiore. In seguito, per il paragone con il sistema classico, si sono utilizzati pellets di *2 mm*.
Infine, le due alimentazioni simulate hanno le seguenti caratteristiche, *FEED 2* presenta composizione tipica dei tagli idrogenati, *FEED 1* presenta invece maggiore concentrazione di A, per testare le prestazioni di conversione.

1. Le analisi hanno riscontrato che il taglio C_4 è sensibile alla variazione di d_M, una diminuzione di diametro dei macro-pori comporta un lieve incremento di selettività a parità di conversione, al di sotto di una certa soglia si ha tuttavia un peggioramento delle prestazioni. Questo è dovuto al fatto che l'effetto della diminuzione di area specifica supera quello dell'aumento del trasferimento di massa, entrambi dati dalla diminuzione di d_M. Questo fenomeno di inversione si verifica per d_M maggiori se il valore di L sarà maggiore, ciò avviene poiché l'effetto di diminuzione dell'area superficiale sarà più marcato. La diminuzione dello spessore L, invece, migliora le sempre le prestazioni siccome diminuisce la lunghezza diffusiva fino ad entrare in controllo cinetico, infatti per L inferiore a 5 *micron* non si ha incremento delle prestazioni (*figure 21*). Quanto detto vale per entrambe le alimentazioni. Si noti tuttavia che in *FEED 1* l'idrogenazione porterà inizialmente ad un massimo nella concentrazione di B (*figure 21,22,23*), invece in *FEED 2*, data la minor concentrazione di A si ha da subito profilo discendente per B, ma allo stesso tempo la conversione di A sarà superiore (*figure 24, 25, 26*). In ultima analisi, per entrambe le alimentazioni, si è riscontrato che è possibile diminuire L fino a 5 *micron* per migliorare le prestazioni, mentre d_M non dovrebbe invece scendere sotto i 20-50 *micron* (*figure 40,41*).
2. Per il taglio C_3 valgono molte le stesse considerazioni fatte al punto precedente, in virtu' delle costanti cinetiche superiori a C_4 di almeno un ordine di grandezza (*table 7* in elaborato), si ha maggiore sensibilità alla variazione di L (maggiore incremento di B diminuendo L), le prestazioni migliorano, per entrambi i *FEED*, anche per L inferiore a 5 *micron* (*figure 27, 30*). Considerando d_M, se L pari a 20 *micron*, si potrà diminuire fino a 50 *micron* prima di incorrere in perdita di selettività, se L di 5 *micron*, potrà essere diminuito fino a 20 *micron* (*figure 28, 29, 31, 32*).
   L a sua volta può anche essere sottile fino a 0.5 *micron* senza che si raggiunga il limite cinetico. Le considerazioni fatte riguardano entrambe le alimentazioni.
3. Per quanto riguarda C_2, come per *figure 33,34,35*, i profili finali sono sostanzialmente diversi rispetto ai tagli precedenti. Innanzitutto la cinetica catalitica è intrinsecamente più selettiva in B (*figure 33,34,35*), la caratteristica principale di questo taglio è che, essendo in fase gassosa, presenti alta diffusività, ciò risulta in una minore sensibilità a d_M ed L, la conversione desiderata è raggiunta con alta selettività. Si ricordi tuttavia che il vantaggio della maggiore diffusività portato dalla fase gassosa è compensato dalla difficoltà pratica nel controllo della temperatura in un tale sistema.
4. In C_4, nel confronto con un reattore a pellets sferici, configurato come in *table 9* nell'elaborato, si è riscontrato che, per un fissato valore di conversione, avremo concentrazione di B maggiore con il monolita, addirittura del 35% per *FEED 1* e del 18.9% per *FEED 2* (*figure 37,38*), la conversione è inoltre maggiore.

5. *In C_2,* il principale vantaggio è dato dalla maggiore conversione (*figure 38*) così da poter risparmiare principio attivo, l'aumento di selettività è inferiore al punto percentuale.
6. (include anche serie 7,8) Considerando ora le perdite di carico, è interessante vedere come per la scelta del diametro dei macro-pori sia anche opportuno tenere in considerazione questo aspetto. Come per *figure 39*, è visibile che nel monolita la caduta di pressione è ampiamente sensibile a L e d_M, quando si ha d_M tendente a zero, le perdite di carico tendono infatti ad infinito. Avremo che, fissando ad esempio L a 2 *micron*, la perdita di pressione sarà inferiore nel monolita, infatti per d_M sopra una certa dimensione, rispettivamente 105 *micron* per C_3, C_4 e 55 *micron* per C_2 (confronto con pellets sferici di diametro *2 mm*). Si fa notare inoltre che il valore della perdita di carico è massimamente rilevante in C_4, e diminuisce di circa due ordini di grandezza in C_2, da ciò si comprende che limitare la perdita di pressione è maggiormente vantaggioso per C_4.

8 Conclusioni

L'idrogenazione selettiva è un processo che presenta severi requisiti di purezza, da ottenersi con la migliore efficienza energetica possibile e soprattutto minimizzando l'uso di fase attiva catalitica. A questo scopo, innovativi supporti monolitici alveolari sono stati considerati in questo lavoro di tesi, al fine di valutare i loro possibili vantaggi. La modellizzazione cinetica e le successive fasi di programmazione e simulazione hanno condotto ai seguenti risultati e considerazioni.
Pareti più sottili e macro-pori di dimensioni inferiori migliorano la selettività nonché la conversione, questo fenomeno è più accentuato nel taglio C_3 rispetto al taglio C_4, i vantaggi sono invece minimi per il taglio C_2, dove, per via del trasporto in fase gas e non liquida, la diffusione non limita la cinetica.
La dimensione dei macro-pori presenta tuttavia limiti inferiori, pori relativamente troppo piccoli comportano diminuzione dell'area specifica il cui effetto negativo supera quello dell'aumento di trasferimento di materia. In secondo luogo, per pori più piccoli, crescono le perdite di carico ed il conseguente dispendio energetico.
Queste ultime, calcolate con correlazioni presenti in letteratura, hanno dimostrato di essere comparabili a quelle dei pellets sferici ed inferiori solo per pareti sottili e macro-pori oltre una certa dimensione.
Il confronto con pellets sferici, in termini di selettività, ha messo in risalto il beneficio dei monoliti in particolare per il taglio C_4. C_2 non presenta invece particolare sensibilità alle *texture properties* del supporto.
Come prospettive per continuare la ricerca, per quanto riguarda il modello, l'uso di correlazioni più complesse per porosità ed area specifica è consigliabile per un miglioramento della qualità dei risultati. In seguito, l'analisi su una possibile diluizione in più *stage* dell'alimentazione dell'idrogeno può portare ad ulteriore ottimizzazione delle prestazioni.
Infine, i bilanci di energia possono essere implementati nel modello, considerando dunque anche sistemi non isotermi e più vicini alla realtà industriale.

1 Introduction

In oil and gas refining industry, selective hydrogenation is commonly operated after a steam cracking step which produces olefins, a high value product, this study focuses on selective hydrogenation of polyunsaturated hydrocarbons to obtain monounsaturated solutions, cuts studied have been: butene, propylene and ethylene, namely: C_4, C_3, C_2 cuts.

C_4, C_3, C_2 hydrogenation units are purification steps for ethylene, propylene and butene. Traces of acetylene, methyl-acetylene (MA), propadiene (PD) and butadiene (BD) are formed in the steam cracking furnaces. Presence of acetylene, MAPD and BD has to be reduced to few ppm quantity (table).

Selective hydrogenation is the main purification process adopted for these cuts.

Highly pure monounsaturated cuts are required for a variety of downstream petrochemical processes, such as production of ethylene glycol, polyethylene, PVC, polypropylene and acrylonitrile.

Hydrogenation is preferably carried out in liquid phase, this is not realized for C_2 cut because it would require a consistent energy expense in order to rise operating pressure.

Fixed bed reactors are commonly adopted, hydrogenation process is operated isothermally or adiabatically, the latter is the most exploited solution in industrial practice (Mohundro, 2003).

Catalysis is exploited to enhance reaction rate and selectivity. Aside economical aspects, material choice for the active sites is based on particle activity and selectivity, palladium (Pd) particles reveal to be the best choice as active sites for the three cuts considered (Thomazeau and Boyer, 2011).

Catalyst performance is also dependent on its texture properties. Catalyst's structure is given by its support, specific area, bulk porosity, skeletal porosity and diffusion length affect selectivity, conversion, internal diffusion limitation and pressure drop along the reactor.

In this study, an innovative approach to selective hydrogenation catalysis is exploitation of highly porous monolith supports, expected to provide high surface-to-volume ratios, efficient mixing of fluids and low pressure drop if compared to commonly exploited support solutions. (Heck, Gulati and Farrauto, 2001). In this work, alveolar structured monoliths, synthetized as HIPE polymers, are considered as innovative approach to selective hydrogenation catalysis.

Alveolar monoliths are solid cell-structured materials characterized by a hierarchical porosity, material inner morphology consists in a repeating unit that can be a hollow honeycomb, sphere or a reticular structure (foams), in the first two cases interconnecting holes are present in the shell wall between hollow spaces so that all the void volume is accessible. Hierarchical porosity results from the hollow shells which constitutes the macro-pores and the channels inside the shell (catalytic wall) which constitutes the second class of pores, usually meso-pores.

Example of hierarchically structured monoliths are PolyHIPE, highly porous emulsion-templated polymers synthesized within high internal phase emulsions (HIPE). This polymers can be generated using Silica (SiO_2) as monomer to obtain a final product, referred as Si(PHIPE) in literature (Destribats *et al.*, 2012), with

porosity in the range 57-92% and Brunauer-Emmet-Teller (BET) surface area between 700-900 m^2g^{-1} (Destribats *et al.*, 2012).

Regarding pores size, Si(PHIPE) can have macro-pores size in the diameter range 20-500 µm with meso-pores in the shell wall of 4-11 nm diameter and narrow size distribution. This innovative material has been chosen for its peculiar textural parameters and used as reference for developing a kinetic model predicting selective hydrogenation performance in a laboratory reactor.

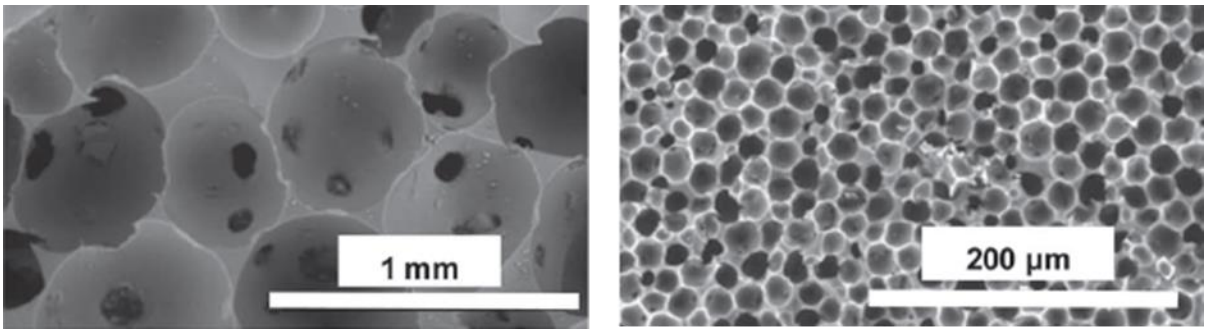

Figure 4: MEB pictures of Si(HIPE) monolith porosity, extreme cases for macro-pores dimension (figure from (Destribats *et al.*, 2012))

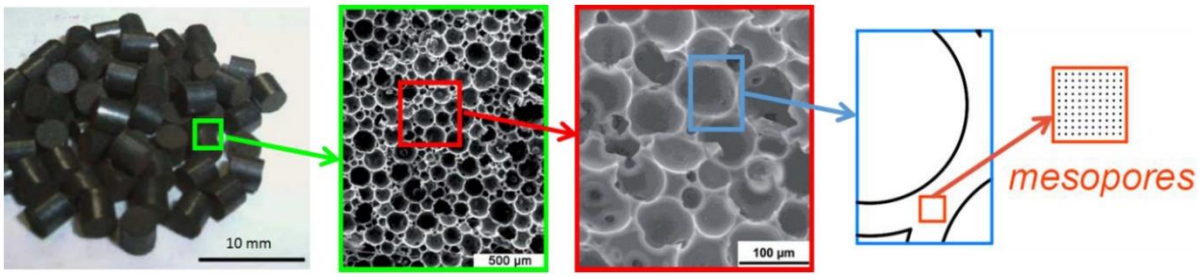

Figure 5: Pictures of monoliths (right), MEB pictures of alveolar monoliths and representation of the wall (figure from (Destribats *et al.*, 2012) with modifications)

The model of the occurring phenomena in the system is built in order to quantitatively evaluate the effect of the various textural parameters. Model derivation and assumptions made are presented, obtained results are exploited to find an optimal monolith configuration.

Parameters analyzed are: wall thickness and bed porosity (void fraction due to the macro-porosity), results for different feed compositions are presented. As a plus, gas-liquid equilibrium (for C_3,C_4 cuts) and pressure drop in the monolith are taken into account.

Finally, comparisons are made with the commonly exploited technologies in industrial practice. Systems considered are fixed bed reactor and pellets string reactor.

Selectivity analysis and comparisons are computed with equal operative conditions, kinetic parameters and diffusion length in the solid catalyst, performance difference between the various systems is assessed to justify monolith exploitation.

2 Motivations and objectives

In a time of sustainability demanding, separation and purification processes play a key role to provide products that respect strict impurities tolerance. In hydrocarbon industry, olefins are taking more and more importance among the high value products of refineries. Highly pure olefin cuts are required to assure safety and quality in the downstream processing. Light olefins demand, especially for ethylene, is in continuous growth, on the other hand even small quantity of polyunsaturated impurities can alter the downstream processing, which is usually a polymerization process, causing drop in final product quality and catalysts inhibition or poisoning, this is why a purification process is essential to reduce impurities to ppm quantity.

Hierarchical alveolar monoliths have been chosen as catalytic materials in order apply innovation in the selective hydrogenation unit operation. A range of experimental results is provided in literature for different pellets-based catalytic systems while highly porous monoliths have been still poorly studied.

Aim of this work is to build a mathematical model of an alveolar monolith to simulate its performance in selectivity and conversion tuning main textural parameters, for a given reaction kinetics, in order to find optimal configurations of the solid in terms of maximal selectivity considering the associated pressure drop. Particularly, Study-case focuses on assessing most important textural features of the monolith to evaluate their impact via mathematical simulation and on the built of the model for future synthesis of catalysts for experimental testing.

3 State of the art

3.1 Refineries

Whether many steps forward have been made regarding exploitation of new sources of energy and consumption goods, crude oil still remain the main raw material to provide commodities and energy. We can simplify refineries structure as divided in three main complex operations, figure 3, crude oil extracted from subsoil is subjected to a first distillation (atmospheric topping), its distillate is then fractionated (cold fractionation), while bottom stream goes into a second column (vacuum topping).

Most cuts coming from these three operations are still processed, this time the aim is not fractionation but transformation of the cut, therefore chemical reactions are involved, the objective is always to maximize fractions which have more interest on the market.

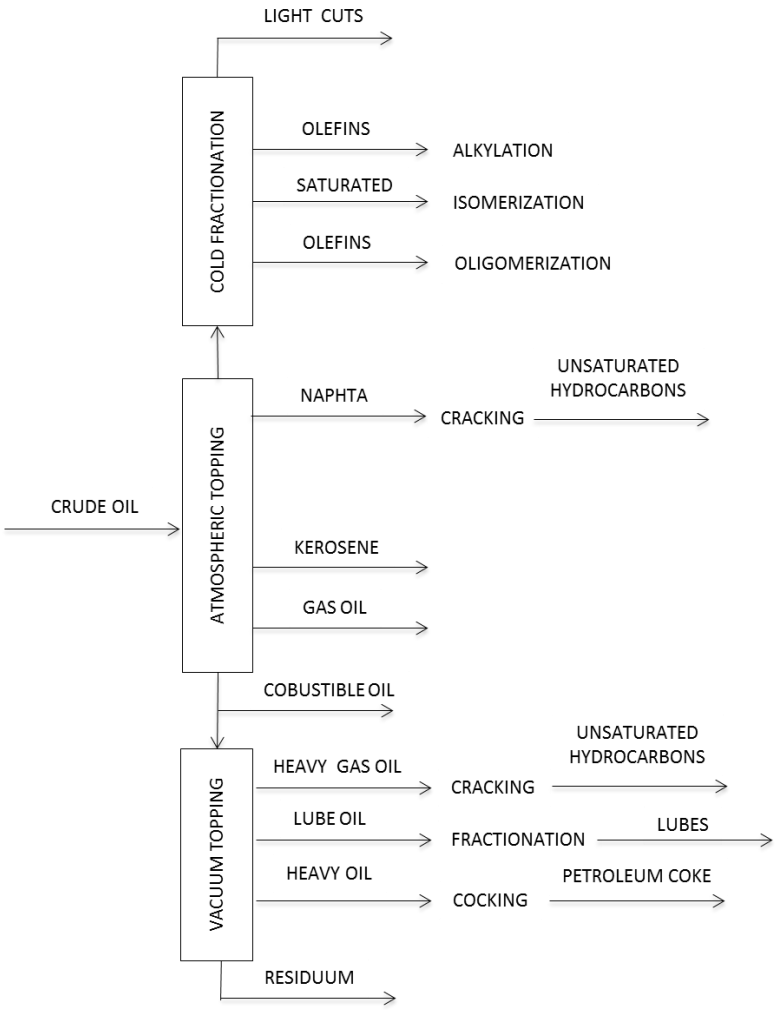

Figure 6: Scheme of crude oil fractioning and first processing steps (upstream refining)

3.2 Cracking

Most of the light olefins produced in refineries come from cracking operations which is performed to obtain lighter products. Main reactions that take place in cracking are:

Dehydrogenation:

$$C_{(m+n)}H_{2(m+n)+2} \rightarrow C_{(m+n)}H_{2(m+n)} + H_2$$

Cracking:

$$C_{(m+n)}H_{2(m+n)+2} \rightarrow C_mH_{2m} + C_nH_{2n+2}$$

After cracking, which is operated in a furnace, via direct or indirect heating, the hydrocarbons mixture is rapidely cooled (quenched); at this point the mixture pass through the separation process in figure 4, realized by columns in series, the first distillation column, also called demethanizer, mainly separates methane and hydrogen which are precious compounds. Next, columns in series separates the cuts of interest, mainly C_2 to C_4.

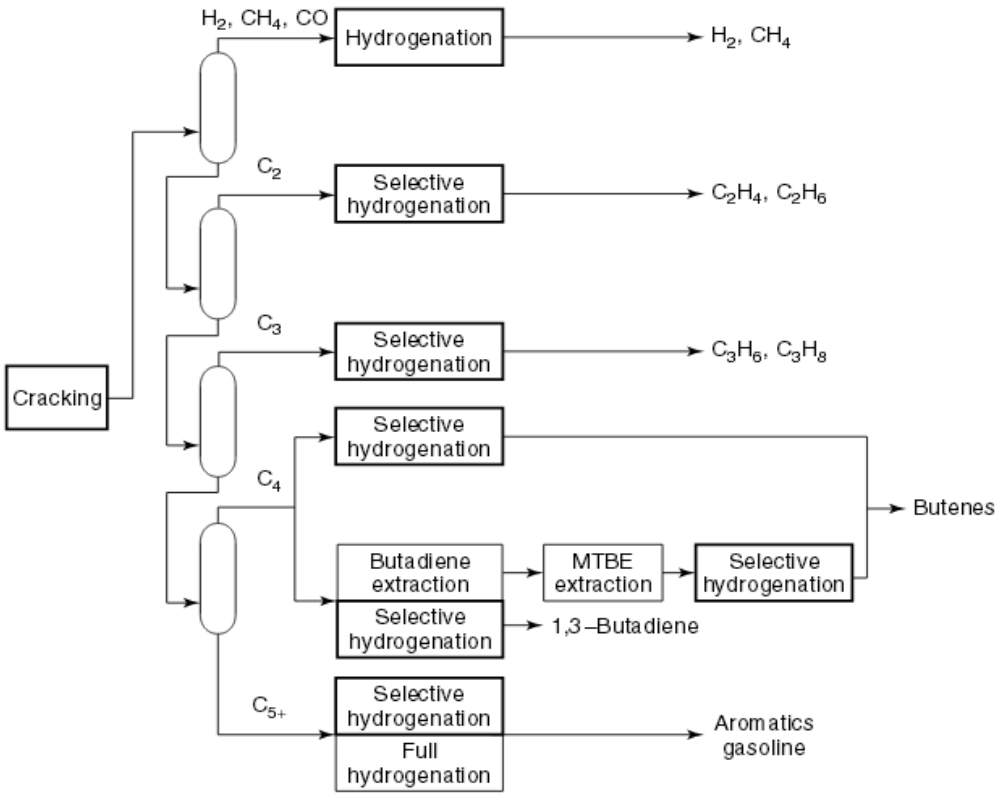

Figure 7: Scheme of downstream treatment of cracker effluents (figure from ('"Hydrogenation Reactions" in: Handbook of Heterogeneous Catalysis', 2008))

Nowadays ethylene is the highest valued product of cracking processes, it is used to obtain high consumption derivatives, including polyethylene and styrene.

Propylene and butene are also outcome of cracking and massively exploited in the downstream industry to produce polipropylene, acrylonitrile, LDPE, co-polymers and fuels.

A minor amount of light olefins (C_2 to C_4) is extracted as well from refinery gases to maximize this high value product.

3.3 Selective hydrogenation

Light olefins are selectively hydrogenated as purification step, this because very low amount of polyunsaturated impurities is demanded before the downstream processing (Thomazeau and Boyer, 2011). This operation assures maximal valorization and exploitability of the cut.

Feed	Impurity	Product of interest	Specification (mass ppm)
Cut C_2	Acetylene	Ethylene	<5
Cut C_3	Propyne, propadiene, methylacetylene	Propylene	<10
Cut C_4	1,3 Butadiene	Butenes	<10

Table 3: Selective hydrogenation specifications for production of intermediaries for petrochemistry (figure from (Thomazeau and Boyer, 2011) with modifications)

Molar fraction			
Feed	**A**	**B**	**C**
Cut C_2	0.014	0.687	0.294
Cut C_3	0.045	0.915	0.050
Cut C_4^*	0.005	0.932	0.063

Table 4: Molar fractions of C_2 and C_4 cuts after cracking and separation steps; A polyunsaturated compound, B monounsaturated compound, C: saturated compound. *cut C_4 composition after extraction of 1,3-butadiene. (figure from (Thomazeau and Boyer, 2011) with modifications)

While for C_2 and C_4 there is no presence of pre-treatment of the cut, in the case of C_4 we have that the stream is subject to previous processing steps, this happens because this cut contains a wide range of compounds different products of interest (1-3 butadiene, butenes). Before going toward selective hydrogenation a fraction of this cut is subjected to 1,3-butadiene extraction because this polyunsaturated compound is used as raw material for synthetic rubbers production (ABS, SBR).

Finally selective hydrogenation process is set up considering that, firstly, reaction is exothermic, thus cooling is needed during reaction or between reaction steps; secondly rate of reaction tend to be fast and therefore more likely to be limited by the physical phenomena of the system than by the intrinsic kinetics.

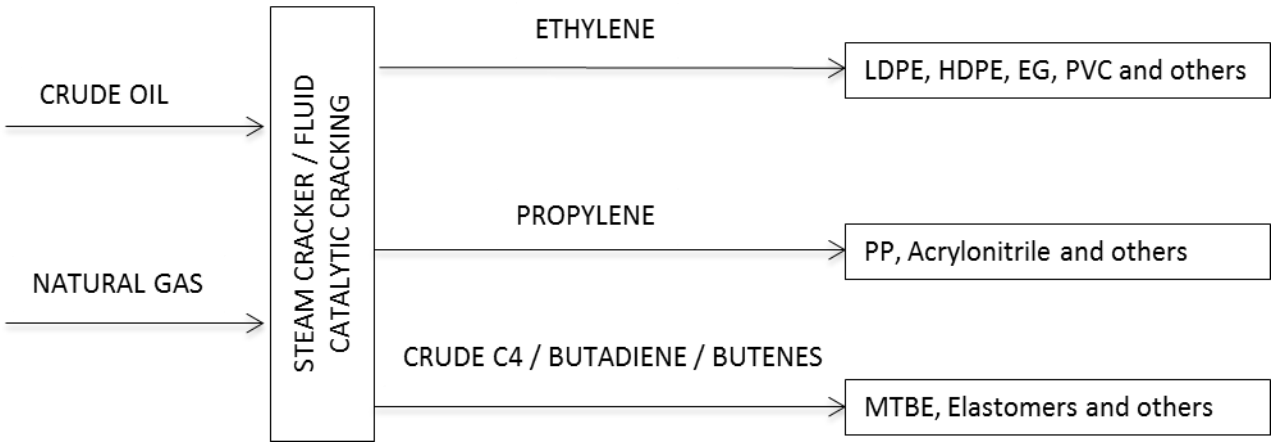

Figure 8: Simplified scheme of olefins value chain

3.4 Catalysis

The modern industrialized world would be inconceivable without catalysts. There is no other technical principle which combines economic and ecological values as closely as catalysis, thus, catalysis is the main technology in chemical industry, catalysis not only boost reaction rate, but also influence selectivity. Majority of all catalytic processes require heterogeneous catalysts, while the remaining fraction includes homogeneous catalysts and biocatalysts (Arnold, Dobert and Gaube, no date).

Selective hydrogenation is tipically performed via heterogeneous catalysts thus we have a catalyst in solid phase and reactants as liquid or gas.

Many solid materials (elements and compounds) including metals, metal oxides, and metal sulfides, are catalysts. Only a few catalytic materials used in industry are simple in composition, e.g., pure metals (e.g. Pd) or binary oxides (such as g-Al_2O_3, TiO_2). Typical industrial catalysts, however, consist of several components and phases. This complexity often makes it difficult to assess the catalytic material's structure.

Solid catalysts may be divided in two families: supported catalysts and unsupported, or bulk, catalysts.

Selective hydrogenation is industrially performed on supported catalysts, in this case the support provides high surface area and stabilizes the dispersion of the active component (e.g. metals supported on oxides).

Aside economic considerations, evaluation of the proper active site material relies on three requisites:

Activity: capacity of decreasing activation energy of the overall reaction by changing the mechanism, assessed according to Sabatier principle, different catalysts activity is typically obtained by volcano plot diagrams. Palladium shows to have the highest activity for diolefins hydrogenation (table 4).

Selectivity: capacity of favorite a reaction path more than another in consecutive or parallel reactions. It depends on adsorption equilibrium between active sites and reactive species, because of adsorption competition, the ratio of adsorption constants for two reactants quantifies the selectivity of the active site. Palladium provide the highest ratio of absorption and is thus used in industry (table 4).

Stability: durability of the catalyst at sufficient effectiveness of activity and selectivity. Stability assesses endurance of the catalyst in term of its capability of being active for a number of cycles. Loss of activity depends on physical loss of active particles or deactivation phenomena.

Hydrogenation of unsaturated hydrocarbons is not fast enough without the presence of a catalyst, its choice does not just rely on its activity, but mostly on its selectivity. Palladium (Pd) has been proven as the best choice for hydrogenation of alkynes and diolefins as shown in table 4, revealing also sufficient poison resistence.

Allumina supports are adopted for Pd in industrial practice, with an active phase loading in the range 0.03-30%, in selective hydrogenation the loading range 0.03-0.5% is used for C_4,C_3,C_2 cuts (Verdier, 2003).

Support geometry commonly consists in beans of diameter 2-5mm, above this range intergranular diffusion problems may appear while lower diameters results in high pressure drop. To minimize impact of internal transfer limitation, thickness of active phase is in the range 0.1-0.3mm on the catalytic particle, thus only a small fraction of particle volume is active. Thin active phase layer minimize diffusion length, diffusion inside the solid, which is lower than external diffusion, is commonly computed from the external one via corrective factors representing porosity and tortuosity (table 3) (Octave Levenspiel, 1999).

Eventually features requested from the support are chemical inertia, for example it has not to catalyze oligomerization or isomerization reactions, then mechanical and thermic resistance.

Catalyst	**Porosity (ε)**	**Tortuosity (τ)**
0.5% Pd on alumina	0.59	3.9
1.0% Pd on alumina	0.5	7.5

Table 5: Porosity and tortuosity factors for diffusion in catalysts (from (Octave Levenspiel, 1999) with modifications)

Compound to hydrogenate	**Activity of the active phase (decreasing)**	**Selectivity to olefins of the active phase (decreasing)**
Olefins	Rh > Pd > Pt > Ni	-
Alkynes	Pd > Pt > Ni, Rh	Pd > Rh, Pt
Diolefins	Pd > Ni	Ni, Pd > Ru > Rh, Pt

Table 6: Activity and selectivity of metallic active phases for hydrogenation reactions (from (Thomazeau and Boyer, 2011) with modifications)

Active phase	**Support**
Ni	alumina / silice
Pd	alumina
Pt	alumina / zeolite

Table 7: Supports coupled with active phase (from (Thomazeau and Boyer, 2011) with modifications)

3.5 Reactors and operating conditions

While continuous stirred reactors (CSTR) are mostly adopted in total hydrogenation, partial and selective hydrogenation are performed in fixed bed reactors. Different configurations are adopted depending on productivity demands: mono or multi-tubular reactor, presence of recirculation, etc.

The system is operated adiabatically or seldom isothermally, operating temperature for light olefins can be from 20°C up to 80°C, it has to be considered that if reactor is instead adiabatic increase of temperature has

to be limited, this is usually obtained through a series of adiabatic reactors with cooling between stages (figure 6).

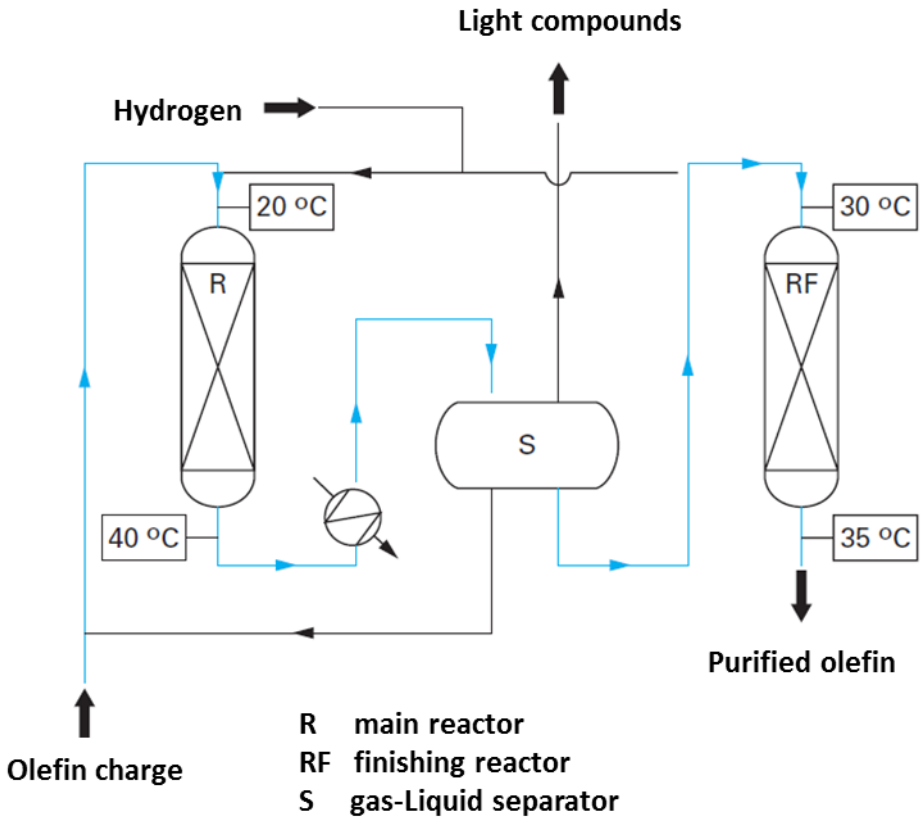

Figure 9: scheme of a selective hydrogenation process for C_3 cut, configuration with two adiabatic reactors (multi-stage) with intercooling and a separation step (figure from (Thomazeau and Boyer, 2011) with modifications)

Because hydrogenation is an exothermic reaction, temperature has to be limited from increasing excessively to keep reaction under control, moreover, chemical equilibrium moves toward total hydrogenation for low temperatures. In order to balance these two phenomena some reactors are cooled in order to have a limited ΔT from inlet to outlet, in this case system may be considered as a series of isothermal reactors operating at different temperature.

Operating pressure usually depends on the previous step, commonly the cuts C_4,C_3,C_2 come from the upstream processing with pressure of 8-10 bar, with the aforementioned temperatures we have presence of liquid phase only for C_4 that is therefore processed in this pressure conditions. C_3 can be processed either in the gas phase or as biphasic, the latter is preferable and requires pressure rise up to at least 20-25 bar, bi-phasic case has been considered in the study. C_2 cut is hydrogenated in the gas phase at upstream pressure considering that a high energy demanding pressure rise would be needed to obtain the liquid phase.

Because we usually want the reaction to be the controlling step in the system, mass transfer between phases has to be relatively fast to avoid influence on the reaction rate, this imposes superficial velocity of the inlet feed in the range 1-10 cm s^{-1}.

Some hydrogenation reactions can be very fast, in such cases rate can be controlled by the rate of external or internal mass transfer. In the first case reactants transport in the liquid-solid interphase limits the conversion, in the second case it is the diffusion in the catalytic pores to limit the conversion.

Whether reactive feed can be operated in gas, liquid or mixed phase, it is preferable to operate in liquid phase because of its higher calorific capacity which allows to reduce thermic gradients and presence of hot-spots which can be also mitigated by vaporization, for a very light cut as C_2 presence of liquid phase would require excessive pressure, so it is processed in gas phase.

Paramount feature to assure inside the reactor is reactants mixing, to have reaction proceeding at rate close to its intrinsic kinetics, hydrogen has to be properly dispersed without formation of bubbles, this is achieved with distributors in the inlet and inside the reactor, as well as with pre-mixing of feeds, mal-distribution also leads to temperature gradients.

Reacting system		**Necessity of recycle for T control**	**Operating condition**
Fixed bed in liquid, gas or mixed phase	Monotubular	Yes	Usually adiabatic
	Multitubular	No	Usually isothermal
	Multistage	No	Intercooled adiabatic stages

Table 8: Choice of reactors for selective hydrogenation (from (Thomazeau and Boyer, 2011) with modifications)

In current technologies hydrocarbon and hydrogen feeds are typically in co-current flow (Alves *et al.*, 2012), and can be circulated in both upflow or downflow mode (figure 7). The former is better to obtain complete catalyst wetting while the latter needs high flow regime so it is more indicated for high productivities. In this study a co-current configuration is used in the model, complete wetting of the catalyst will be considered, because hydrostatic pressure is neglected the reactor could be operated both upflow or downflow.

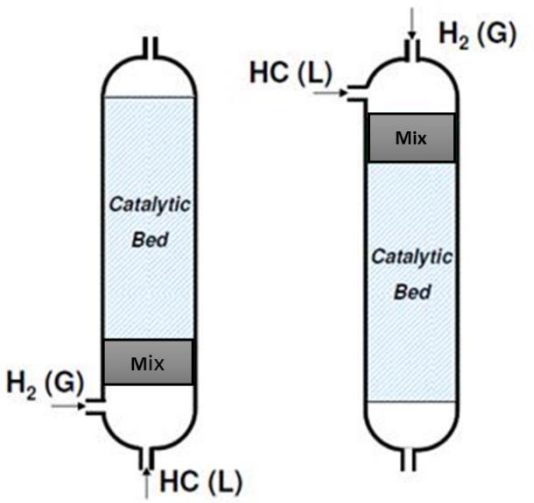

Figure 10: upflow and downflow scheme for fixed bed hydrogenation reactor

3.6 Innovative monolithic materials

A monolith is a unitary structure, the ones adopted in catalysis are composed of inorganic oxides or metals with texture similar to a honeycomb. The monolith is structured with uniform sized and parallel channels or with open cells, section of these can be of any shape. Currently, monoliths made their way into catalysis and they are preferred to pellets shaped catalysts in many applications (mainly environmental). Advantage of these structures is low pressure drop, due to a large open frontal area and high bed porosity, as well as high surface to volume ratio and good thermal conductivity.

On a monolith support, active phase is can be also deposited with an ulterior carrier, deposition techniques are the ones typical of heterogeneous catalysis (wash-coating, impregnation, electrodeposition).

Alveolar monoliths are an innovative example of structures applicable to catalysis, these are formed by void interconnected shells and they are characterized by a hierarchical porosity. A first class of pores, macro-pores with a diameter of a few to hundreds of micron, is given by the void shells, then a second class of pores exists inside the walls of the shells, the latter are meso-pores with size of a few nanometers developing a total surface area of 700-900 m^2g^{-1} (Destribats *et al.*, 2012).

Alveolar monolith's void fraction can be much greater than pellets catalysts, this because the 'repeating unit' of the structure is a hollow shell of permanent shape instead of a pellet. Shell walls can be thin down to a few micron so that internal diffusion resistance is significantly reduced.

A breakthrough in alveolar structured monoliths is represented by polyHIPEs (Destribats *et al.*, 2012)these are porous emulsion-templated polymers made within high internal phase emulsions (HIPEs). An emulsion is a two-phase mixture of immiscible fluids in which one is dispersed in the

Second in the form of droplets, a suitable surfactant is commonly required to

stabilize the droplets dispersed in the continuous phase.

HIPEs are paste-like high viscous emulsions, foam-like on the micro-scale and with high inner void volume. HIPEs can be used as templates to generate different polyHIPEs, a method to synthesize innovative monoliths with a narrow bi-modal distribution of the pores is to use sol-gel processing to deposit an inorganic material, like Silica, at the outer of HIPE droplets.

Bi-modal structure is the key to obtain high porous catalysts with low pressure drops, high surface area and limited internal diffusion resistance.

Innovative polyHIPE research is hence broadening the number of potential applications and an industrial "breakout" in the fields of porous supports seems to be around the corner (Silverstein, 2014).

3.7 Alveolar monolith synthesis via sol-gel process

To generate materials with such architecture, non-aqueous emulsions and surfactant-stabilized aqueous emulsions are adopted (Destribats *et al.*, 2012), subsequently a monolith is synthetized as a porous organic polymer.

The sol–gel process is a technique to yield a solid material (a gel), built starting from molecular precursors via the formation of colloidal particles (sol) which polymerize into a solid structure.

Condensation of precursors (via cross-linking reactions), typically alkoxides, induced by the controlled addition of water represents the beginning of the process, then a network is built via nucleation and growth of sol particles. A variety of parameters (presence of salts, concentration of the solution, pH) can be tuned to define the final network morphology and pore structure.

Final removal of the solvent after solidification of the network determines structure porosity.

To yield a bi-modal distribution of pore size in the solid, it is necessary to combine liquid/liquid phase separation and sol–gel processing, while phase separation is responsible of macro-porosity (alveoli), the polymerization of precursor produces the meso-porosity.

In order to use HIPE in the preparation of monoliths, the precursor (sol) is added to the continuous phase (aqueous solution for the synthesis of monoliths), then gelation is triggered.

Next, the dispersed phase is removed leaving a macro-porous structure. To generate meso-pores a structure-directing agent is added to the sol.

Eventually, because of HIPE morphology (droplets of different size), interconnections (quasi-spherical holes) between macro-pores are formed in the contact areas between droplets during sol-gel synthesis after phase separation, these are of paramount importance because they allow fluid flow through the whole monolith void space, thus allowing its employment as support.

Example of alveolar monoliths obtained combining HIPE and sol-gel process are silica macro-cellular foams labeled as Si(PHIPE) (Destribats *et al.*, 2012; Silverstein, 2014)

Once we have the availability of such effective support an active phase can be placed on it (i.e. metallic particles). Metal particles can be inserted onto a preformed monolith by immobilization of precursor into the previously formed porous material. To do this several techniques used for other catalysts can be adopted, such as impregnation, electrodeposition or wash-coating.

Solid	Porosity [%]	Skeletal density [g cm^{-3}]
$Si(PHIPE)_{64H}$	73	0.97
$Si(PHIPE)_{70H}$	74	1.02
$Si(PHIPE)_{75H}$	80	0.98
$Si(PHIPE)_{80H}$	78	1.05
$Si(PHIPE)_{85H}$	83	1.02
$Si(PHIPE)_{90H}$	92	1.10

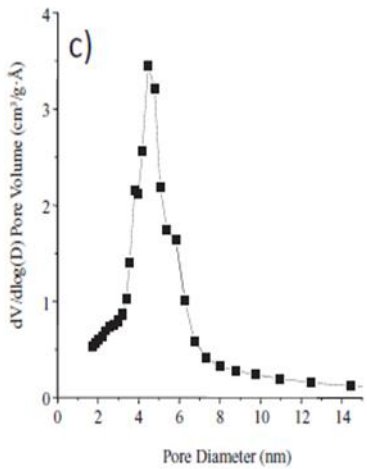

Figure 8: Porosity of Si(PHIPE) alveolar monoliths (left), example of meso-pore size distribution for alveolar monolith $_{2.6}Si(PHIPE)_{85H}$ (right) (from (Destribats *et al.*, 2012))

In conclusion, we can summarize that hierarchically organized porous monoliths can be prepared via sol-gel method combined with templating strategies. While the meso-porosity, in the final monolith, is related to the sol-gel process, the macro-pores formation is instead caused by the templating agent (Feinle, Elsaesser and Hüsing, 2016). The texture of the final monolith can be described in the simplest way possible by its two main features, macro-pores average diameter (d_M) and the thickness of its walls (2L) as showed in figure 10.

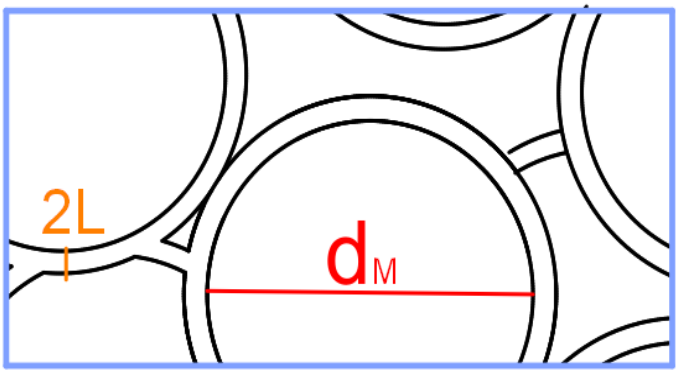

Figure 9: simplified texture of an alveolar monolith synthetized as polyHIPE

4 Model

4.1 Assumptions

In order to develop a kinetic model of the system, before writing down the equations it is essential to formulate the assumptions on which the system is built.

Model assumptions:

- Plug flow model for gas and liquid phase
- Absence of radial dispersion
- Steady state operating conditions
- Constant volumetric flow of the liquid phase
- Isothermal and isobaric system
- Co-current flow of reactants in up-flow mode
- Complete wetting of the catalyst surface
- Reacting feed at G/L thermodynamic equilibrium
- Gas phase has ideal behavior

Ulterior assumptions regarding feed composition:

- Absence of CO
- Absence of sulfuric compounds
- Simplified composition for C_4 cut after 1,3 Butadiene and MTBE extraction

The fixed bed reactor is modeled as an ideal plug flow reactor (PFR), thus there is no axial dispersion and no radial or angular gradients, hence the system behavior is assumed to be mono-dimensional. Finally, the equations are written in steady state condition and liquid volumetric flow is approximated as constant.

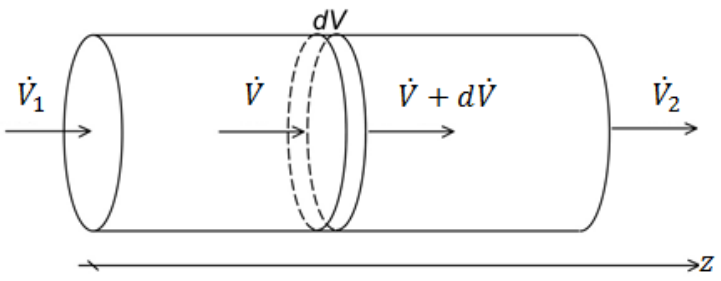

Figure 110: Scheme of plug flow reactor model

Despite selective hydrogenation is commonly carried out in adiabatic systems, preferred to isothermal where a refrigerant is needed (Mohundro, 2003), this case study focuses on isothermal solution, this is the simplest

modeling choice, it allows to neglect energy balances and give a fixed value to kinetic constants so that mass transfer sensitivity to the texture of the catalyst can be put on focus.

Complete wetting of the catalyst surface is assumed in this system, thus if we have a bi-phasic stream we will have that catalytic surface is only in contact with liquid phase, there is no gas-solid interface.

This will be the case for C_4 cut where we have a three-phase system and as well for C_3, in fact if pressure is above 20 bar with temperature around 40°C liquid phase is formed, we thus decided to simulate the process at 25 bar (Samimi *et al.*, 2014). For C_2 cut liquid phase is not present because it would require prohibitive (T,P) conditions (pressure above 130 bar if temperature is fixed to 40°C).

Finally, inlet feed, if bi-phasic, is considered to be at thermodynamic equilibrium with the gas phase so to have a starting distribution of compounds between the phases before entering in the reactor. The gas phase, which contains mostly hydrogen, follows ideal gas behavior.

Figure 11: Scheme of complete wetting(left) and partial wetting(right) for the interfaces in a three-phase system

4.2 Kinetic equations

Inside the system, C_4, C_3, C_2 cuts can be subject to a number of reactions where isomerization reactions are also involved. These multiple reactions scheme can be lumped into a simpler kinetic mechanism if we only consider the degree of unsaturation of the compound.

We adopted a simplified consecutive reaction scheme:

- C_4 reaction:

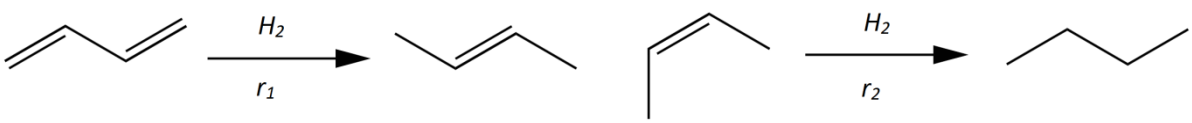

- C_3 reaction:

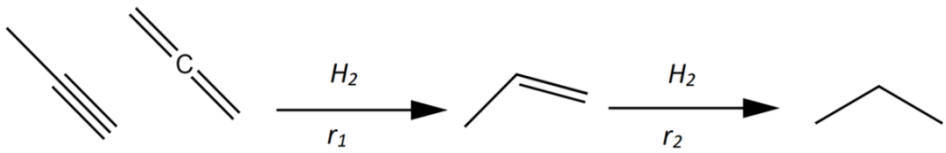

- C_2 reaction:

General reaction scheme:

$$A \xrightarrow[r_1]{H_2} B \xrightarrow[r_2]{H_2} C$$

Figure 12: Reaction scheme for hydrogenation of polyunsaturated compounds

Where:

A is the polyunsaturated hydrocarbon

B is the monounsaturated hydrocarbon

C is the saturated hydrocarbon

4.3 Reaction Mechanism

Reaction takes place on palladium active sites, to describe the kinetics of the system, the Langmuir-Hinshelwood-Hougen-Watson (LHHW) approach for heterogeneous catalysis is largely used in literature to write kinetics expressions (Arnold, Dobert and Gaube, no date).

Regarding adsorption, Langmuir model approximates the surface of a catalyst as an array of equivalent active sites which do not interact either before or after chemisorption, only a mono-molecular layer can be adsorbed on the surface, on which, mass action law is valid and reversible.

The fraction of saturation of the active sites due to adsorption is expressed as direct function of partial pressures or concentrations in the fluid phase by means of Langmuir adsorption coefficients.

For derivation of rate equations, reaction mechanism is analyzed and elementary kinetic expressions are derived. The mechanism can be always divided in three main steps:

Step 1: A molecule is adsorbed on an active site on catalyst surface

Step 2: The molecule reacts with another on an adjacent site or with one coming from the fluid stream, as well it can simply decompose while on the site

Step 3: The molecule is desorbed from the active site on catalyst surface

Subsequently the expressions are combined assuming that the system is in steady state condition.

The obtained kinetic expression always bulky even for the simple reaction mechanism we adopt (figure 13). Hence, to simplify the final expression one reaction step is assumed as rate determining while the others are considered to be almost at thermodynamic equilibrium.

Kinetic expressions assume the following generalized aspect:

$$R_i = \frac{KF^{*}DF}{RT^{exp}} \qquad \textbf{(4.1)}$$

Where:

KF = kinetic factor

DF = Driving force

RT = Resistance term

This is the most used approach to express reaction rates in selective hydrogenation of hydrocarbons [Bressa, Samimi], lumping two sets of experiments available in literature (Alves *et al.*, 2012; Bos *et al.*, 1993), we adopted the following reaction rates expressions:

$$r_1 = \frac{k_1 x_A x_{H_2}}{1+K_A x_A+K_B x_B} \; ; \; r_2 = \frac{k_2 x_B x_{H_2}}{1+K_A x_A+K_B x_B} \qquad \textbf{(4.2)}$$

Where x_i are molar fractions.

The kinetics expressions don't consider presence of adsorption competition and adsorption constant of hydrogen is neglected.

4.4 Mass balance equations

After a set of assumptions, fluid dynamics and transport properties also need to be assessed before writing down the equations. Process conditions, bed geometry, operating variables and fluid physical properties are instead established.

Both fluid phases follow plug-flow model, the axial dispersion is neglected and isothermal conditions are considered. Cross section is considered to be the same monolith cylindrical section which volume is correspondent to reactor volume.

Textural properties of the material are considered to be homogeneously distributed in the system, thus catalyst physical parameters describe the average characteristics of the system.

As a result, monolith performances will be function of its macro-pores diameter and wall thickness, analysis are therefore performed varying the values of the two parameters (which are consequence of the synthesis of the material).

Void porosity (also referred as bed porosity) of the monolith is also expressed as sole function of macro-pores diameter and wall thickness.

Macro-pores have been assumed to be perfectly spherical, while the wall is ideally considered as a slab. Physical properties of the fluid have been evaluated using DIPRR database available in *IFP Energies Nouvelles* resources. Correlations for mass transfer between phases and interphase areas are taken from literature (Alves *et al.*, 2012).

Control volume is, as stated, the cylindrical monolith volume that is modeled as a three-phase system, this is divided into cylindrical cross sections of infinitesimal thickness 'dz' so that in every infinitesimal volume the whole set of material balance equations is solved until the total reactor length is reached.

Before assessing and solving reactor's equations, material balance inside the catalytic wall has to be considered, its equations are obtained considering transport phenomena inside the wall as governed by Fick's law for diffusion transfer, with no convective transfer and no accumulation term, the material balance in the catalytic wall is shown in equation.

$$\boldsymbol{D_{e,i}C\frac{\partial^2 x_i}{\partial y^2} = \rho_w r_i} \qquad \begin{cases} \boldsymbol{x_i(y=L) = x_{iS}} \\ \boldsymbol{\frac{dx_i}{dy}(y=0) = 0} \end{cases} \tag{4.3}$$

$$\boldsymbol{i = A, B, C, H_2}$$

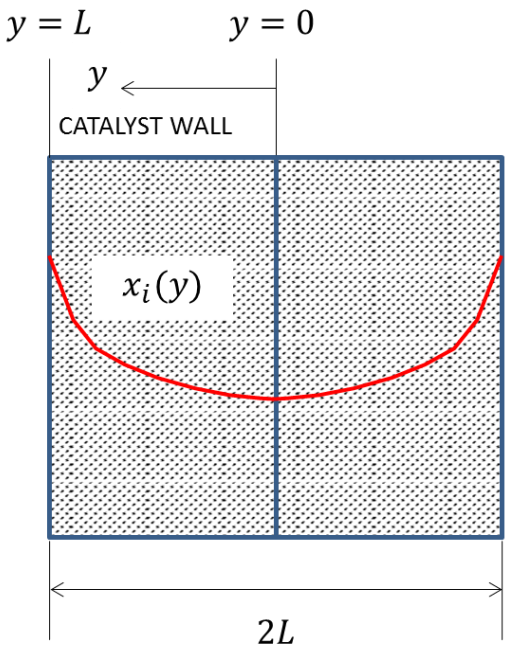

Figure 13: Graphic representation of molar fraction profile inside the wall

Equation 3 consists in a set of boundary value problems (BVP), we need in fact to assess a boundary condition for each extreme of integration, hence the extremes are y = L that represents wall surface and y = 0 that is the center of the wall where meso-pores end is reached. Boundary conditions are expressed as Dirichlet conditions. For the wall's center (y = 0) we assume to have a flat profile for the molar fraction, hence null derivate, on the other hand, regarding wall's surface, we give the molar fraction value, because this value is not known as parameter, it will be calculated iteratively for every step in the computational algorithm, as it will be discussed subsequently.

Now it is possible to express system equations, they can be divided into two groups, the first set of equations (equation 6,7) solves the balances of an infinitesimal volume of thickness 'dz' for every compound, these equations will be named micro-kinetics equations. An ulterior set of equations updates properties values, namely molar concentrations and volumetric flowrates (latter only for gas phase), these equations can be referred as macro-kinetics equations, the overall system is schematically depicted in figure 15.

Because three phases are present in the system, mass transfer takes place for two interphases.

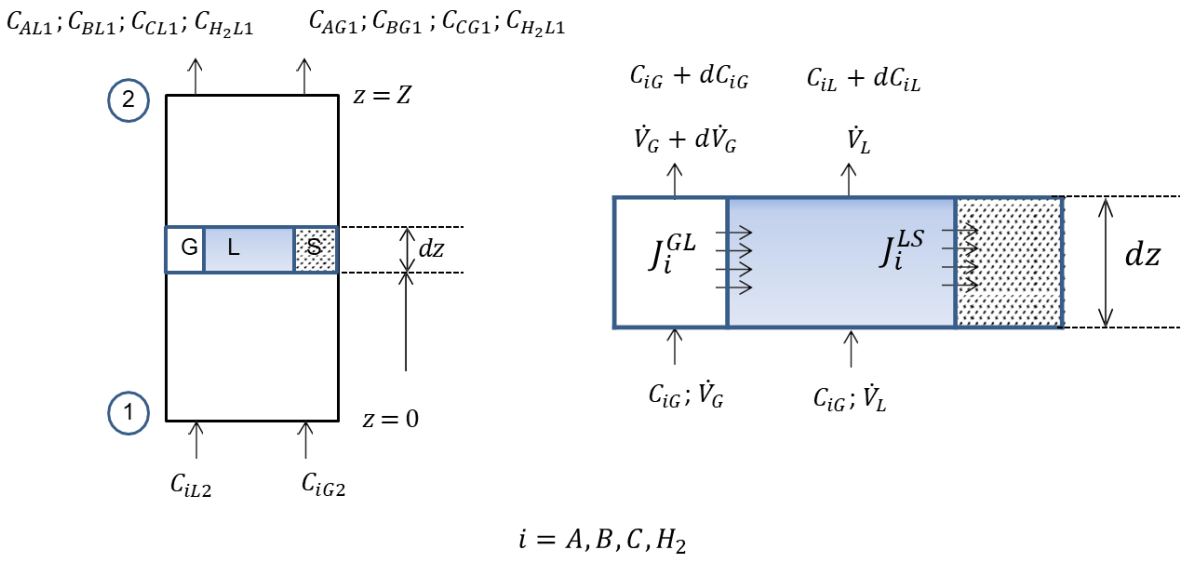

Figure 14: Three-phase reactor graphic representation, overall reactor (left), infinitesimal volume (right)

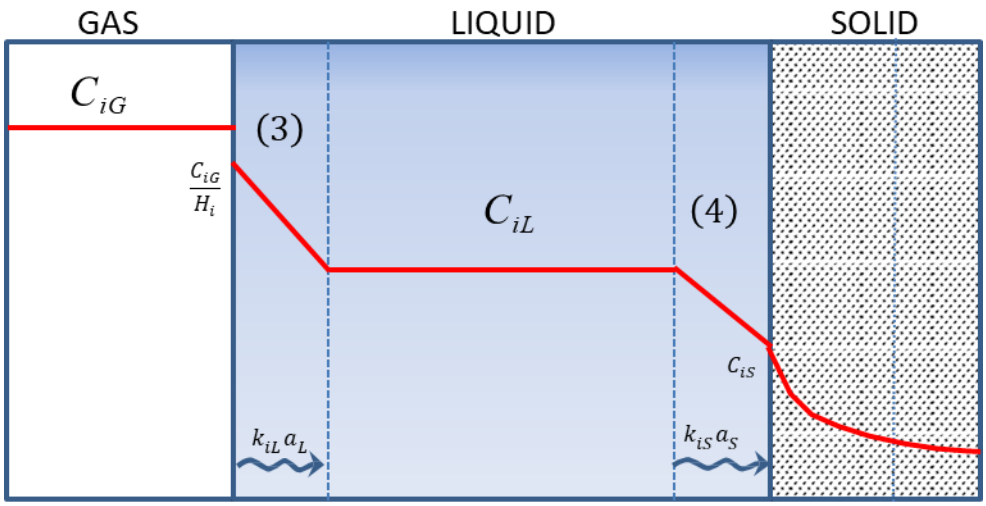

Figure 15: Interphase mass transfer representation

Equations associated with figure 15 are:

Macro-kinetics equations (8 equations):

$$\textbf{(1) GAS :} \quad C_{iG}\frac{d\dot{V}_G}{dz} + \dot{V}_G\frac{dC_{iG}}{dz} = -J_i^{GL}aS \tag{4.4}$$

$$\textbf{(2) LIQ :} \quad \dot{V}_L\frac{dC_{iL}}{dz} = J_i^{GL}aS - J_i^{LS}aS \tag{4.5}$$

Micro-kinetics equations (8 equations):

$$\textbf{(3)}\ J_i^{GL}aS = k_{iL}a_LS\left(\frac{C_{iG}}{H_i} - C_{iL}\right) \tag{4.6}$$

$$\textbf{(4)}\ J_i^{LS}aS = k_{iS}a_SS(C_{iL} - C_{iS}) = \rho_w\eta R_{iS}(1-\varepsilon_B) \tag{4.7}$$

Where: $i = A, B, C, H_2$

In micro-kinetics, represented on the right in figure 15, we have two inter-phase mass transfers, species are transported only via diffusion mechanism. In equation 4.3, diffusion in the liquid film is balanced with the average reaction rate (expressed in terms of surface reaction rate and an effectiveness factor). For simplicity, graphic representation follows film theory as transfer mechanism in figure 16. Correlations actually used for mass transfer consist in semi-empirical formulas (Bressa *et al.*, 2003; Giani, Groppi and Tronconi, 2005), these will be discussed in the next paragraph.

4.5 Parameters derivation

Expressions for surface areas and mass transfer coefficients comes from literature (Alves *et al.*, 2012; Giani, Groppi and Tronconi, 2005). They are here divided in two groups, first one reports interphase transfer from the liquid phase to the monolith solid surface, the second one gives correlations for alumina-coated spherical pellets, performance gap between pellets technology and the innovative monolith will be outcome of these expressions adopted from literature since comparisons in selectivity use the same amount of total active phase in the system.

A third set of expressions reports mass transfer between gas and liquid phases, this is not dependent on the catalyst used, thus the same correlation is adopted.

Liquid to Solid transfer:

- Monolithic catalyst:

- $k_{iS} = \frac{D_i}{d_s}(1.1Re^{0.43}Sc^{0.33})$

- $a_{iS} = \frac{{d_M}^2\pi - [{d_{conn}}^2 N_{conn}\pi/4]}{[(d_M+2L)^3 - {d_M}^3]\pi/6}$

- Spherical beans catalyst:

- $k_{iS} = \frac{D_{iL}}{d_h} \times \begin{cases} (Sc_{iL})^{1/3}(1000d_{ps} - 2.2)\,; & Re_{Lm} < Re_c \\ 550(Sc_{iL})^{1/3}Re_{Lm}^{0.14}d_{ps}\,; & Re_c < Re_{Lm} < Re_s \\ 0.75(Sc_{iL})^{1/3}Re_{Lm}^{0.5}\,; & Re_{Lm} > Re_S \end{cases} \quad \begin{cases} Re_{Lm} = (u_L\rho_L d_h)/\mu_L\,; \\ Re_c = 0.312\exp(341d_{ps}); \\ Re_s = 7.77\exp(334d_{ps}); \end{cases}$

- $a_{iS} = \frac{6}{d_{sp}}(1 - \varepsilon_B)$

Gas to liquid transfer:

- $k_{iL} = \left(\frac{1}{k_{iGf}} + \frac{1}{k_{iLf}}\right)^{-1} \quad ; \quad k_{iGf} = \frac{0.4}{[1+(\rho_V\rho_L)^{0.5}]^{0.5}}\left[\frac{g^2(\rho_V\rho_L)^{0.5}}{\mu_L\rho_L}(D_{iG})^3\right]^{1/6} \quad ; \quad k_{iLf} = 16.95\frac{D_{iL}^{0.5}\xi_{VL}^{0.1}\sigma^{0.6}}{(1-\frac{\varepsilon_L}{\varepsilon})\rho_L^{0.2}}$
- $a_{iL} = 2.36\frac{(1-\frac{\varepsilon_L}{\varepsilon})\,\rho_L^{0.2}\xi_{VL}^{0.4}}{\sigma^{0.6}}$

Monolith bed porosity () is to be considered as the bulk void fraction of the reactor, it is expressed as function of wall thickness (2L) and macro-pores average diameter (d_M). Assuming void fraction can be computed through a simple geometrical correlation, this has been expressed as the ratio between void volume of the hollow sphere (diameter is the one of macro-pores) and the volume of the sphere extending its ray by half wall thickness (L) and subtracting the average volume of interconnecting pores. Plugging a constant number

of two connection per macro-pore, and a diameter of the connection equal to one tenth of macro-pore's one values of bed porosity coherent with what reported in figure 9 where obtained so to confirm the reliability of the correlation.
For a fixed bed of spherical pellets instead, bed porosity can be assumed as a constant value not depending on the diameter of the spheres (Octave Levenspiel, 1999).

Monolithic catalyst:

- $\varepsilon_B = \frac{{d_M}^3 \pi/6}{[(d_M+2L)^3\pi/6] - L{d_{conn}}^2 N_{conn}\pi/4}$

Spherical beans:

- $\varepsilon_B = 1 - \pi/6$

Diffusivity coefficients values are taken from literature (Bressa *et al.*, 2003). To solve the boundary value problem (BVP) provided by the wall balance, an 'effective' diffusivity coefficient value is used in the solid, this is computed starting from component bulk diffusivity coefficient via equation 4.4.

$$\boldsymbol{D_{i,e} = \frac{D_{iL}\varepsilon_w}{\tau}} \qquad \textbf{(4.8)}$$

Where τ is tortuosity and ε_W is the wall porosity or skeletal porosity.
A constant average value has been plugged for the two parameters, for every catalyst considered, 0.59 for the former and 3.9 for the latter (Octave Levenspiel, 1999), considering for 0.5% Pd on alumina as in table 3.
Wall density (ρ_w), or skeletal density, in equation 4.3 has also a constant value, considering the silica monolith $_{2.3}$Si(PHIPE)$_{90H}$ a density of 1000 kg m^{-3} has been adopted (Bressa *et al.*, 2003).
At this point, considering equation 4.9, effectiveness factor (η) is computed in the calculation algorithm without using simplified correlations provided by literature but directly from its definition Equation 9.
To compute the integral reaction rate has been calculated in 100 points from y = L up to y = 0.

$$\boldsymbol{\eta_i = \frac{\int_L^0 R_i(y)}{R_{iS}L}} \qquad \textbf{(4.9)}$$

Eventually, volumetric flow rate of the gas phase ($\dot{V}_G$) is considered following the ideal gas behavior as in equation 10.

$$\boldsymbol{\dot{V}_G = \frac{\dot{n}_G RT}{P}} \qquad \textbf{(4.10)}$$

5 Computational algorithm

As discussed in the previous paragraphs, model developed consists in a set of differential and algebraic equations (DAE) which constitute the molar balances of the system and that are expressed as function of the molar concentrations.

In a separate script, pressure drops are computed via algebraic equations (Bressa *et al.*, 2003; Giani, Groppi and Tronconi, 2005). The molar balance on macro-pores wall, consists instead in a set of second order differential equations with boundary conditions at the two ends (BVP) as by equation 4.3.

First, operating conditions are plugged as global variables, then follows an iterative routine consisting in two loops as in figure 17.

The internal loop provides solution of the BVP set iteratively, starting with an initial approximation for surface concentrations (C_{iS}), the external loop update values for the next infinitesimal reactor volume (position z + dz), using the stated equations of the balance, until reactor length (Z) is reached.

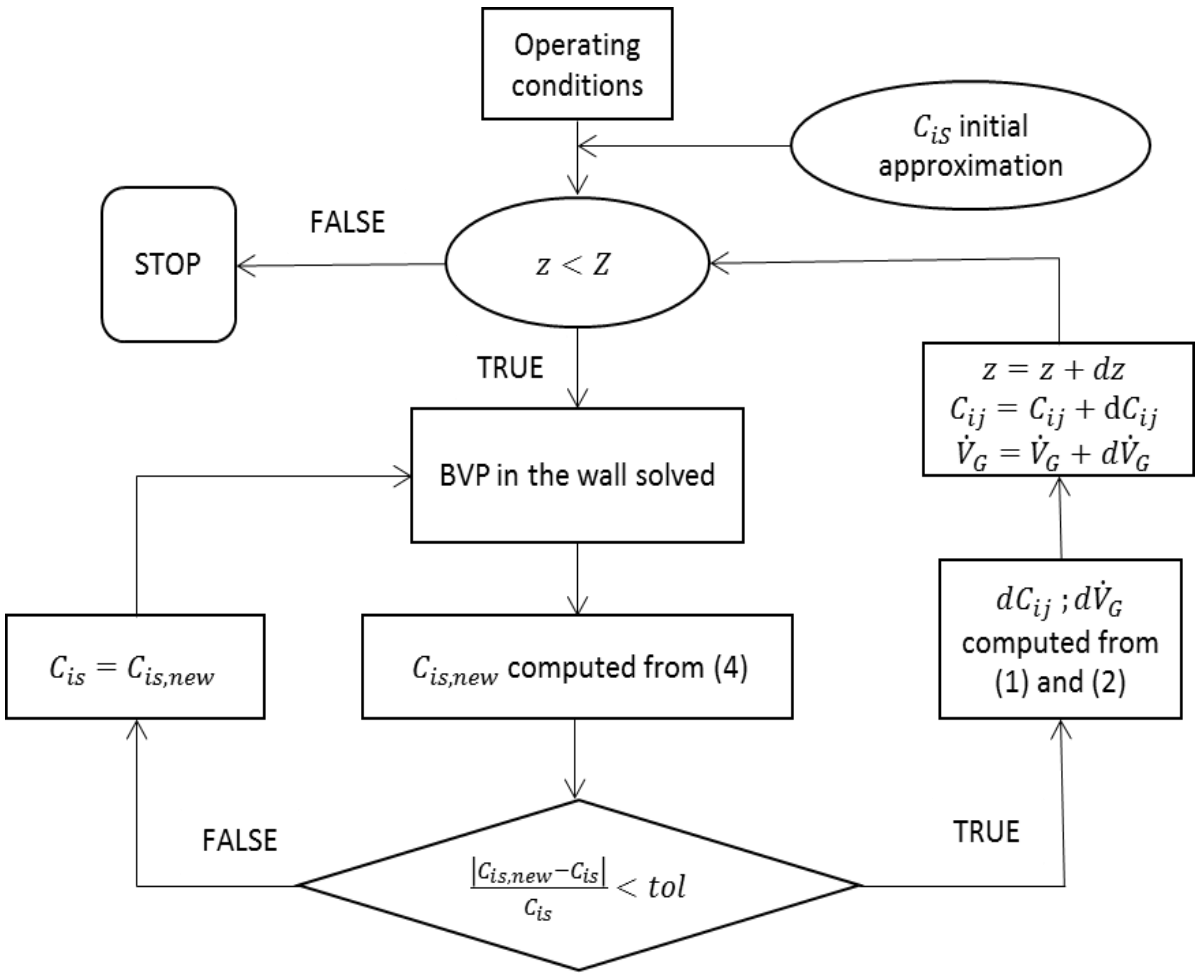

Figure 16: Schematic representation of the calculation algorithm coded on MATLAB

5.1 BVP solution

To solve the BVP, MATLAB tool bvp5c is exploited, this solver is a finite difference solver code that implements a collocation formula (four-stage Lobatto formula). The collocation polynomial provides a continuous solution with no angular points that is fifth-order accurate. The formula is implemented as an implicit Runge-Kutta formula. To apply the solver, the equations have to be reduced to first order differential equations, thus it is required to double the number of equations.

In conclusion, MATLAB provides another BVP solver tool named bvp4c, this follows the same syntax of bvp5c, calculation routine only differs in the evaluation of error while reaching tolerance. While in bvp4c error is evaluated indirectly, bvp5c has direct estimation of the error being hence more accurate.

5.2 DAE solution

Set of differential equation is solved via MATLAB without use calculation of tools, equations are typed in their explicit expression and differential term is computed. Algebraic equation (4) is exploited to update surface concentration values for BVP boundary conditions, while the differential equations (1)(2) are solved to update parameters for the next infinitesimal volume of reactor (position z + dz). Effectiveness factor present in (4) is calculated after BVP solution by computing reaction rate in several points (100) within wall thickness, summing the rates we have a value for the integral term and factor can be computed from equation 4.9.

5.3 Pressure drop computation

A correlation to calculate pressure drop in alveolar monolith has been taken from literature, because poor study has been undertaken on the subject an expression used for solid foam catalysts has been adopted (Giani, Groppi and Tronconi, 2005).

Hydrostatic variation of pressure is neglected because we want to focus on performance difference between alveolar monoliths and spherical pellets catalysts, thus only dynamic pressure drop is accounted.

Bi-phasic fluids require different correlations compared to mono-phasic, this because presence of two phases in a flow requires more complex expressions, in fact friction also takes place between the phases and the contribute of each phase to the total pressure drop is not linear hence Ergun equation cannot be used for two phase flow. Regarding spherical pellets fixed bed the gradient of pressure is here computed adopting a literature correlation (Bressa *et al.*, 2003) that considers a bi-phasic flow in spherical pellets, this expression is adapted to evaluate drop in monoliths using another literature source (Giani, Groppi and Tronconi, 2005). The assumption made to achieve a pressure drop profile for bi-phasic flow in the monolith is that the same friction factors ratio is present between monolith and pellets in a bi-phasic stream as it was in the mono-phasic.

Within the cuts tested, for C_2 we have a mono-phasic flow for which only Ergun correlation is adopted (Octave Levenspiel, 1999). Ergun equation is valid for a wide range of Reynolds numbers, for the bi-phasic streams which are the cuts C_4 and C_3 the aforementioned sources and assumptions are implemented.

C_4, C_3 cuts pressure drop correlations

Spherical pellets:

- $\frac{\Delta P}{Z} = \frac{2 f_{VL} \rho_V u_V^2}{d_h}$
- $f_{VL} = \exp(8 - 1.12 \ln w - 0.079 ln^2 w + 0.0152 \ln^3 \mathrm{w})$

With:

- $w = Re_V^{1.167} \, Re_L^{-0.767}$
- $Re_i = (u_i \rho_i d_{sp})/\mu_i \quad i = L, V$
- $d_h = equivalent\ particle\ diameter$

Monolith:

- $\frac{\Delta P}{Z} = \frac{2 f_{VL} \rho_V u_V^2}{d_h}$
- $f_{VL} = (f_M/f_P)\exp(8 - 1.12 \ln w - 0.079 ln^2 w + 0.0152 \ln^3 \mathrm{w})$

With:

- $w = Re_V^{1.167} \, Re_L^{-0.767}$
- $Re_i = (u_i \rho_i d_M)/\mu_i \quad i = L, V$
- $d_h = d_M$

C_2 cut pressure drop correlations

Spherical pellets:

- $\frac{\Delta P}{Z} = \left(\frac{2f}{d_{sp}}\right)\rho u^2$
- $f_P = \frac{1-\varepsilon_B}{2\varepsilon_B^3}\left[1.75 + 150\left(\frac{1-\varepsilon_B}{Re_m}\right)\right]$

Monolith:

- $\frac{\Delta P}{Z} = \left(\frac{2f}{d_M}\right)\rho u^2$
- $f_M = \left(0.87 + \frac{13.56}{Re_m}\right)\left(\frac{1}{1-G(\varepsilon_B)}\right)^4 \frac{G(\varepsilon_B)}{4}$

With:

- $G(\varepsilon_B) = 2\left[\frac{1-\varepsilon_B}{3\pi}\right]^{0.5}$
- $Re_m = \frac{\rho_m d_p u}{\mu_m}$

6 Results

To start, BVP solution was object of computation, the sole wall balance has been solved to assure that kinetics and internal diffusion in the meso-pores were properly computed to give composition profiles which assured selectivity and appreciable reaction rate as well as for wall thickness sensitivity and model testing. Kinetic parameters of rate expressions are adapted from catalytic tests available in literature (Bos *et al.*, 1993; Bressa *et al.*, 2003) which were performed on commercial Pd/Al_2O_3 catalysts.

To compute the BVP with bvp5c in MATLAB, Dirichlet boundary conditions were given assuming a value for surface concentration.

From sensitivity analysis, impact of wall thickness on molar fraction profile has been evaluated for the cuts.

Parameter	**Value**			**Measure unit**
	C_4	**C_3**	**C_2**	
Surface molar fraction				
XaS	0,09	0,09	0,22	-
XbS	0,75	0,75	0,52	-
XcS	0,04	0,04	0,01	-
XhS	0,12	0,12	0,25	-
Kinetic constants				
k1	1,574	13,83	1,64	kmol / (kg * s)
k2	6,76E-02	0,6287	3,3E-03	kmol / (kg * s)
Adsorption constants				
Ka	1500	1500	3047	-
Kb	75	75	6,1	-
Operating conditions				
T	313	313	313	K
P	10	25	10	bar

Table 9: BVP problem variables and parameters, C_3 cut processed with higher pressure to have a bi-phasic flow

6.1 Catalytic wall profiles

6.1.1 C_4 hydrogenation wall profile

Solving the second order differential equation (equation 4.3) with its boundary conditions the profile of molar fraction, or concentration, is obtained. Sensitivity analysis has been carried out on wall thickness L for all the cuts. It has to be considered that having a condition at both ends have effect on the final profile that has to adjust to satisfy the imposed condition.

Outcome of simulation shows that averagely higher molar fraction is observed for a thinner wall (figure 18), this will result in better exploitation of the catalyst in the overall reactor hence more conversion and higher selectivity due to lower depletion of A in the end of the meso-pore (y = 0).

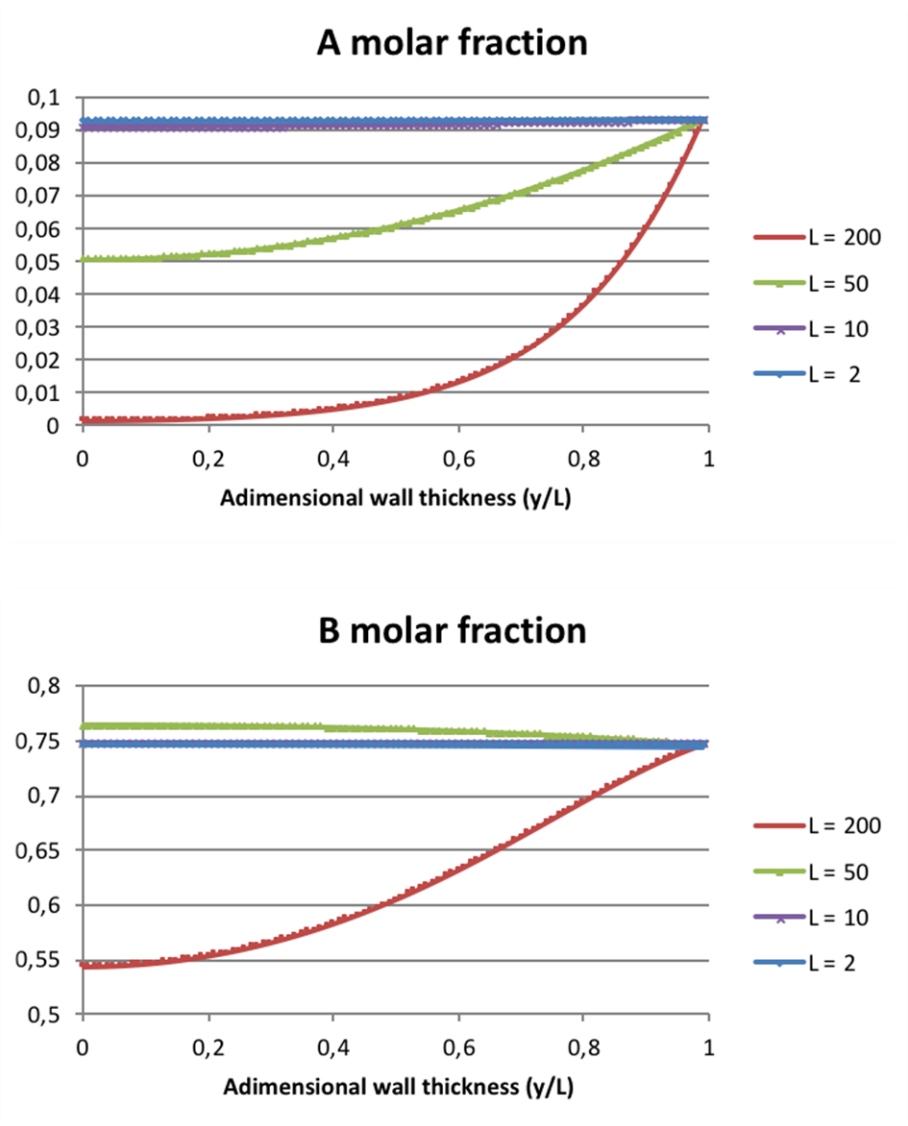

Figure 17: A and B molar fraction wall profile in C_4 for different wall thickness (2L), wall surface is for y/L = 1

Considering that selectivity in B has to be assured, it is understood that smaller values of L are the ones which provide an increasing profile in B molar fraction, an ulterior analysis has been undertaken to probe profile of component B for low L values.

As seen from figure 19, we can see that trend of B profile is sensible to L, being B the middle product of a consecutive reaction its profile can have positive or negative trend depending on the length of meso-pores. If concentration of A is relatively too low, then reaction A→B rate cease prevailing on reaction B→C rate. For L = 75 we can see that profile reaches a maximum at a certain length of the meso-pore, then it decreases

because A concentration becomes too low ending to prevail on the high ratio of the adsorption constants. For L=50, with the surface concentrations given in input we have the profile with higher B concentration, this profile is not to be associated with higher selectivity (and activity), in fact the more profiles are close to be flat the better the performance that will be less limited by diffusion resistance.

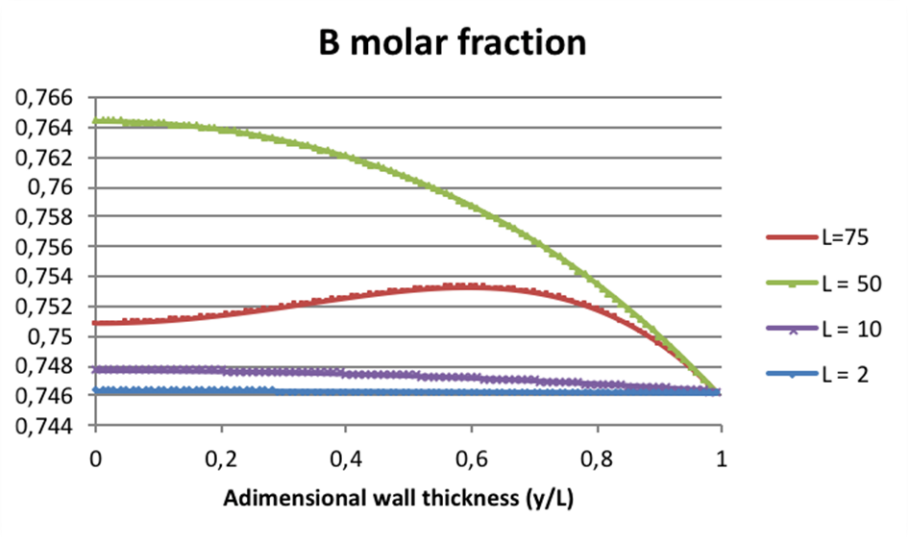

Figure 18: B molar fraction wall profile for C_4, wall surface is for y/L = 1

6.1.2 C_3 hydrogenation wall profile

Because hydrogenation kinetics is faster than for butadiene, polyunsaturated compound A is quickly consumed, this leads to a drop of selectivity toward B, in this case the drop is due to the fact that with the tested surface concentration we have that A is depleted after a certain length.

Highest percentage of A as possible as to be hydrogenated (only a few ppm of polyunsaturated elements are tolerated in the product), but total depletion of A leads to a sudden loss of B, thus catalyst textural parameters and reactor length have to be properly tuned for this purpose as well as hydrogen pressure in the reacting feed.

For C_3 we can probe that diffusion limitation is slightly more sensible to L (figure 20), this can be noticed from A profile by the fact that A depletion reaches 0.04 in the center of the wall (end of the pore) while in the case of C_4 we had 0.05.

This result, considering that diffusion coefficients are not changed, is explained by the faster kinetics that play the role of making the equation more sensible to integration length and thus diffusion limitation plays a more important role on selectivity than in C_4 case.

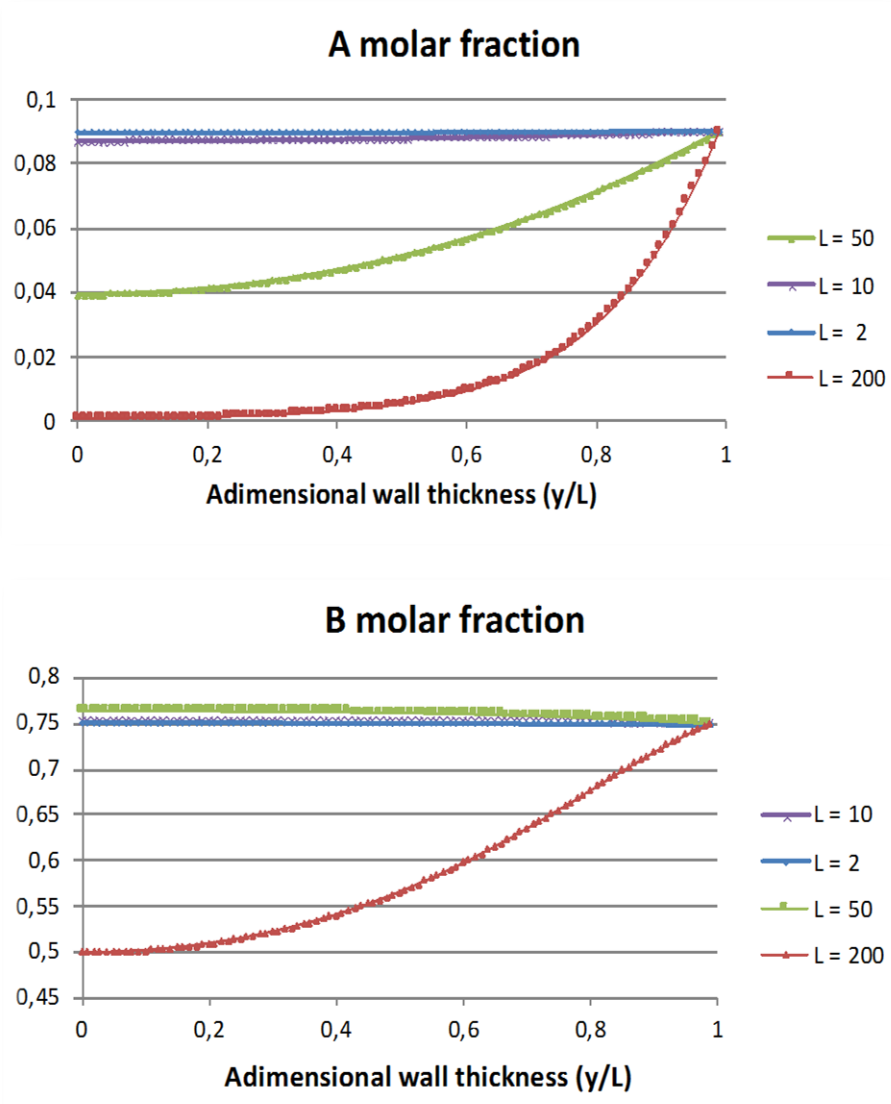

Figure 19: A and B molar fraction wall profile for C_3

6.1.3 C_2 hydrogenation wall profile

Unlike C_4,C_3 this hydrogenation is operated in the gas phase, although a different formalism for the kinetic expressions was adopted in the beginning following literature (Bos *et al.*, 1993), kinetic has been finally lumped with same formalism of the previous cuts, kinetic constants values are adapted from the already adopted literature reference (Bos *et al.*, 1993) in order to fit with the formalism proposed (Bressa *et al.*, 2003). As previously, adsorption constant of hydrogen is not taken into account, molar fractions in reaction rate expressions are obtained from partial pressures supposing ideal gas behavior of the cut.

Being in gas phase, if compared to the previous cuts, C_2 is characterized by a higher diffusion coefficient (around two orders of magnitude) at the interphase with the catalytic wall, this results in lower diffusion limitation that makes the wall thickness L less effective than in the previous cases, this also because adopted kinetic constants are not faster than the previous compounds, if kinetics would be much faster, than the effect of high diffusion could be molded resulting in higher sensitivity to the diffusion length as from C_3 to C_4.

Because we have here a very high ratio of the kinetic constants (k1/k2 = 500) profiles also shows high selectivity in B that has very low tendency to react even for very low concentration of A, for this reason the process is intrinsically very selective.

Even if starting concentration are different than in the previous two cases profiles are comparable and two features can be noticed.

Higher diffusion and kinetic constants ratio are responsible for the profile obtained in C_2 cut, figure 21. Molar fractions are less sensible to wall thickness change, in fact for L = 50 we still have a flat profile of the compound. Finally, because of the kinetics we see that even for L = 200 profile of B shows accumulation of the compound until the end of the pore, proving the intrinsic selectivity of the reaction.

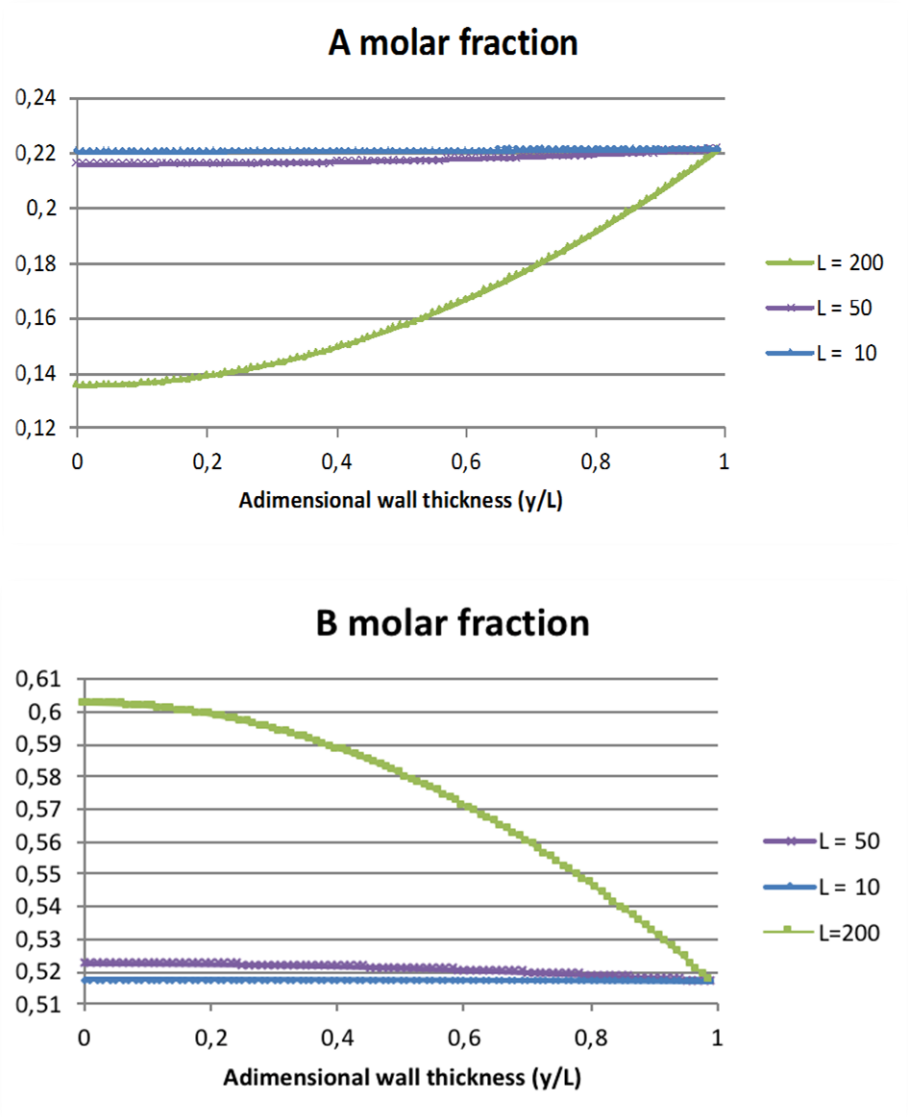

Figure 20: A and B molar fraction wall profile for C_2

6.2 Overall reactor profiles

In view of future experiments on a reactor with laboratory dimensions, the effect of monolith textural parameters in selective hydrogenation of polyunsaturated traces in C_4,C_3,C_2 cuts has been analyzed.

Overall mole balance of the three-phase fixed-bed catalytic unit operated in up-flow mode has been computed, a series of simulations has been used to perform sensitivity analysis.

First screening regards wall thickness effect at constant parameters, then macro-pores diameter, range of calculation was limited by numerical issues during the convergence or by computation time. Finally, comparisons with common fixed bed application has been made running ulterior simulations with parameters adapted for representing a spherical particles catalyst, always keeping the same total load of active phase.

It is fundamental to state that aim of the simulations is to qualitatively probe how parameters, mainly textural ones, influence the system in order to depict the optimal monolithic solution.

Optimal solution for industrial needs consists in the one maximizing selectivity at constant active phase load, secondly, pressure drops are also an important factor to be kept in consideration, therefore pressure drop computation is also included in the model by a separate computation script to be used in parallel with the main algorithm.

It is important to clarify that because in the model we have that monolith void fraction (bed porosity) has been expressed as function of both macro-pores diameter and wall thickness via geometrical correlation, thus, we have a wide range of values for the void fraction which happens to be very sensible to these two parameters. Because active phase load as to be equal in every simulation, the same bed porosity value has been always kept just in equation 4.7, this means that the same amount of catalytic active phase is virtually loaded in every infinitesimal volume dV.

In the following pages, selectivity calculated is defined as toward product B and referred to reagent A (equation 6.1). Selectivity is computed for a fixed outlet A concentration in %wt where 1,E-02 %wt (0.01%wt) corresponds to 100 mass ppm, and 1,E-03 (0.001%wt) is equal to 10 mass ppm which can be considered as the objective of cut purification (table 1) to be adopted for selectivity comparison.

Because desired final conversion was not always reached by the simulations, especially for textural parameters characterized by high diffusion length, most comparisons are made for 0.01%wt of A, keeping in mind that if reactor length would be increased in order to obtain higher conversions, the performance gap would always increase.

$$S_B = \frac{C_{B2} - C_{B1}}{C_{A2} - C_{A1}} \qquad \textbf{(6.1)}$$

6.2.1 Simulations

For each cut, a series of simulations have been run which included: first set to evaluate sensitivity on wall thickness (2L) and a second set testing sensitivity on macro-pores dimension (by diameter d_M).

For C_4, C_3 the two sets have been computed for two feed compositions.

The first one reproduces the composition used in the previous work and it has been simulated to guarantee results continuity, the second one (table 8) is instead a typical feed composition found in industrial practice before hydrogenation of the cut as shown in table 1 (Thomazeau and Boyer, 2011).
Main different between the feeds is in the molar fraction of polyunsaturated compound A which is lower in the industrial composition (FEED 2), this will result in two contrasting phenomena.
First, depletion of A to lower %wt is reached at same reactor length, so that for the length chosen final A of 10 mass ppm is often reached even for the less performing textures. Second aspect is that lower selectivity is to be expected from FEED 2, as will be showed in the profile we have in fact that for FEED 2 decrease in B concentration occurs from the inlet while for FEED 1, B concentration increases reaching a maximum before dropping because of A depletion.

Parameter	**Cut**					**Measure unit**
	C_4		**C_3**		**C_2**	
Mass fraction	FEED 1	FEED 2	FEED 1	FEED 2		
w_{A1}	11,8	0,5	18,1	4,2	1,3	%wt
w_{B1}	85,5	93,0	79,7	90,6	67,7	%wt
w_{C1}	2,7	6,5	2,2	5,2	31,0	%wt
Feed H_2	16	16	24	24	2.4 (bar)	mol/s

Table 10: Composition of inlet feeds simulated

In each case, reactor is dimensioned as a laboratory/pilot reactor with diameter of 0.58 m and length of 2.30 m, flowrate fixed to 3.45 L/s (Bressa *et al.*, 2003), as rate sufficient to guarantee 1 cm/s of superficial velocity of the fluid in the catalytic bed which is the minimum recommended in industrial practice (Thomazeau and Boyer, 2011). Moving on, operating temperature is fixed at 313K (44°C) (Bressa *et al.*, 2003) with absolute pressure of 10 bar, the higher pressure of 25 bar has been adopted solely for C_3 to have a two-phase stream (Samimi *et al.*, 2014; Thomazeau and Boyer, 2011).

6.2.2 C_4 hydrogenation reactor profile

- **FEED 1:**

Selectivity toward B has more sensibility toward wall thickness (2L) when L is above 20 micron, from 50 down to 5 micron a considerable improvement is shown in the results with macro-pores diameter d_M fixed at 100 microns (figure 22). Sensitivity is evaluated by the difference in B concentration with fixed final amount of A impurity. Smaller L is shown to be desirable to maximize B, a 7.4% increase in selectivity is seen with L tuned from 50 to 5 micron for a fixed A final concentration of 0.01%wt, no further increase in selectivity is appreciable from 5 to 2 microns, this is due to internal diffusion that cease being a limiting phenomenon.

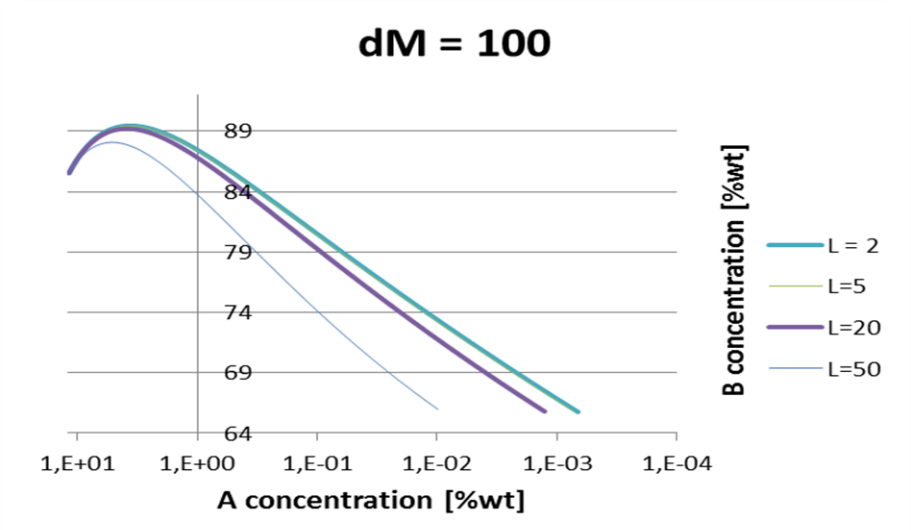

Figure 21: C_4 wall thickness sensitivity FEED 1

For a fixed A final concentration of 0.001%wt an improvement of 1.6% is observed for L going from 20 to 5 micron.

Considering that the total amount of active phase (Pd) in the reactor is constant in every simulation, the gap in performances depends on internal diffusion (if L is varied) and on external mass transfer (if d_M is varied), the latter is related to liquid-solid mass transfer which is given by catalyst surface area and liquid-solid mass transfer coefficient, these two are both function of d_M.

The downstream effect of d_M has been studied in another series of simulations that has been performed keeping L constant at 5 microns.

Slight improvement of 1.8% more B in the outlet is obtained if we move d_M from 300 to 50 micron, this for A final concentration of 0.01%wt, an increase of 2.2% is instead evaluated for 0.001%wt of A at the outlet.

Further decrease of d_M doesn't lead to significant change in performances (while it is leads on the other side to significant pressure drops as it will be discussed) this is a consequence of surface area computation. Even if liquid-solid mass transfer coefficient is higher for smaller pores we got that if ratio d_M /L is not high enough, surface area significantly decrease for smaller pores, thus, here we have that the two phenomena compensate each other so performance doesn't change for d_M from 50 to 5 micron (figure 23).

For a wall thickness fixed at 20 micron (figure 24), competitive effect of surface area and mass transfer coefficient is more appreciable, for d_M from 300 to 100 micron selectivity (with 0.01%wt of reactant left) is enhanced by 0.8% but if d_M gets smaller specific area drop overcomes mass transfer, thus computing profile for d_M of 5 micron a loss of 3.7% is evaluated with respect to 100 micron.

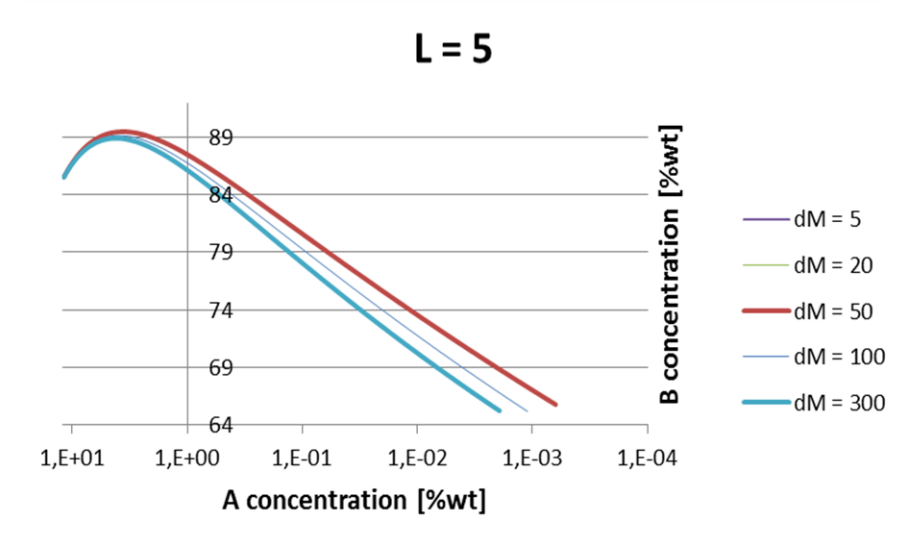

Figure 22: C_4 macro-pore size sensitivity for L = 5 micron; FEED 1

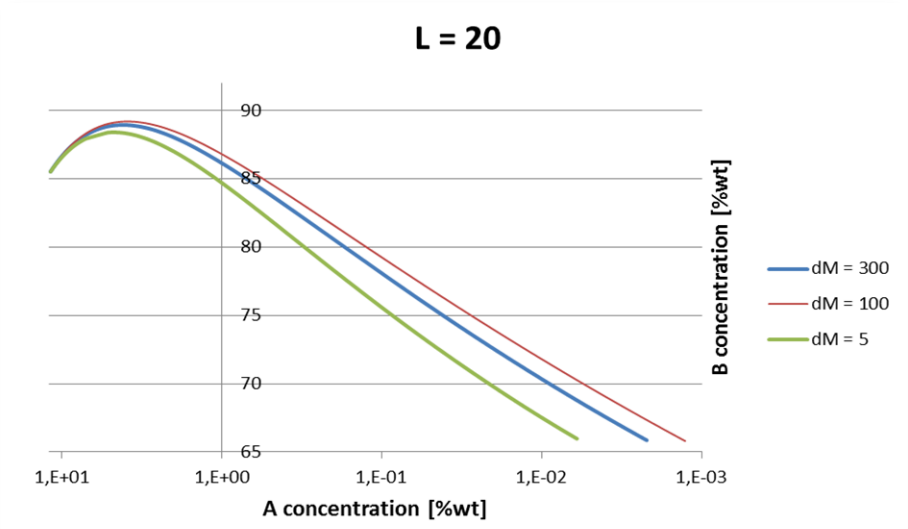

Figure 23: C_4 macro-pore size sensitivity for L = 20 micron; FEED 1

- **FEED 2:**

Industrial composition has lower amount of A in the inlet, as a consequence B doesn't reach a maximum before decreasing, however depletion of A is pushed much further for the same reactor length.

Comparing to FEED 1 we have an higher gain in B by moving L from 50 to 5 micron, in fact we have 8.8% gain (figure 25) compared to the 7.4% obtained with the previous feed in figure 22, both computed for 0.01%wt. Moreover for L smaller than 5 micron, as before, further improvement is neglectable.

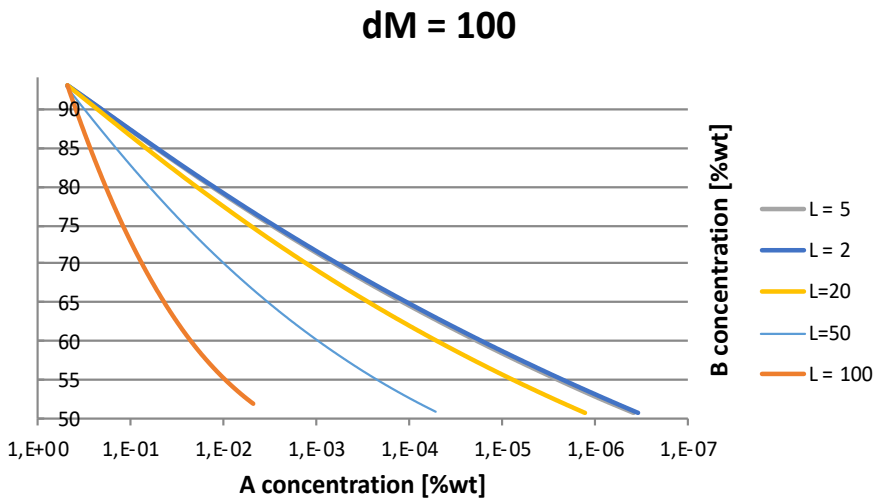

Figure 24: C_4 wall thickness sensitivity; FEED 2

Regarding sensitivity on the macro-pore size, again a 2.6% more B for dM from 300 to 50 micron (figure 26), which is higher than the 1.8% of the previous case, always for 0.01%wt of A. As previously, no improvement if d_M is further decreased due to the effect of balancing between surface area and mass transfer coefficient.

The sensitivity with fixed L of 20 micron (figure 27) again confirmed sensitivity decrease for d_M under 100 micron due to surface area drop.

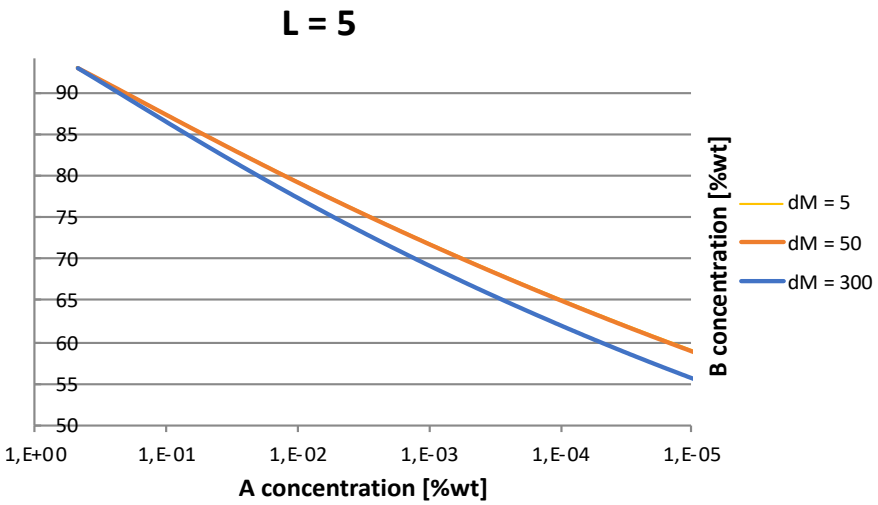

Figure 25: C_4 macro-pore size sensitivity for L = 5 micron; FEED 2

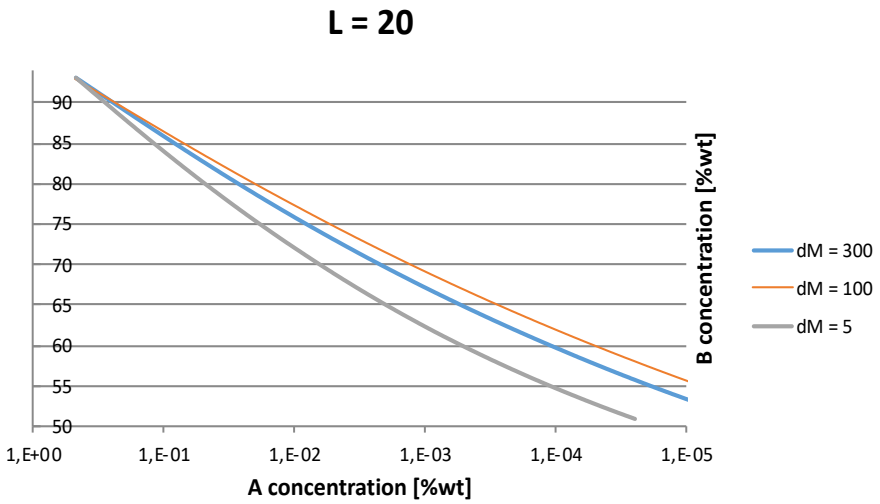

Figure 26: C_4 macro-pore size sensitivity for L = 20 micron; FEED 2

6.2.3 C_3 hydrogenation reactor profile

- **FEED 1:**

C_3 cut presents faster kinetics and slightly different initial composition plugged, simulation results shows higher sensibility to wall thickness (figure 25), for L = 50 selectivity is significantly lower than for the other settings, decreasing L from 20 to 0.5 micron 18.6% more B is resulted for final A of 0.01%wt, whether for final A of 0.001%wt we have a 4.5% improvement for L from 5 to 0.5 micron.
The results confirmed what deduced from the BVP profiles (figures 18,20) that showed more sensitivity to L for C_3 cut.

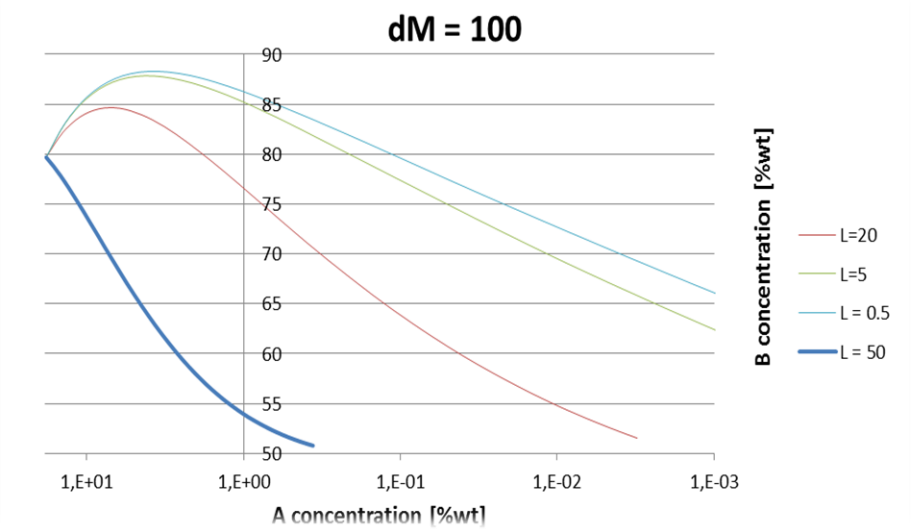

Figure 27: C_3 wall thickness sensitivity; FEED 1

Effect of macro-pore size change was first evaluated for L of 5 micron (figure 26), such wall half-thickness has been chosen because it is the highest value of L which provides sufficient conversion of A for the constant reactor length plugged.

Finally, L of 20 micron has been plugged with values of d_M smaller than 100 to test, as for C_4, if a performance increase is possible or if surface area drop will take over.

Compared to C_4 cut, C_3 cut has faster kinetics that results in higher conversion along the reactor, for L of 5 micron, outlet B for 0.001%wt is increased by 8.4% for d_M from 100 to 20, however if d_M is further decreased to 5 micron selectivity drops due to the major surface area lost, resulting in 11.1% drop from 20 to 5 micron of diameter.

Regarding L of 20 micron (figure 27), increasing d_M under 100 micron proved to slightly improve selectivity, but as d_M is further lowered to 20 performance get worse, however gain in selectivity for d_M from 100 to 50 is 1.3% more B.

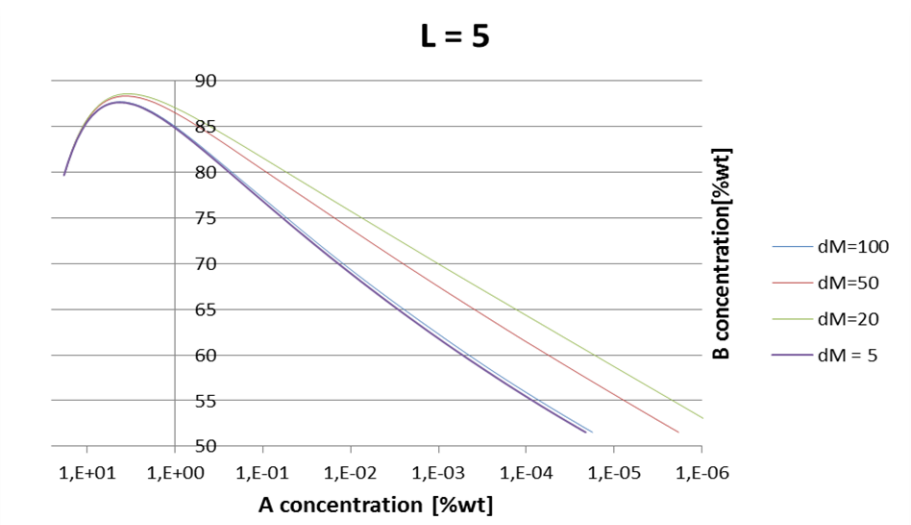

Figure 28: C_3 macro-pore size sensitivity for L = 5 micron; FEED 1

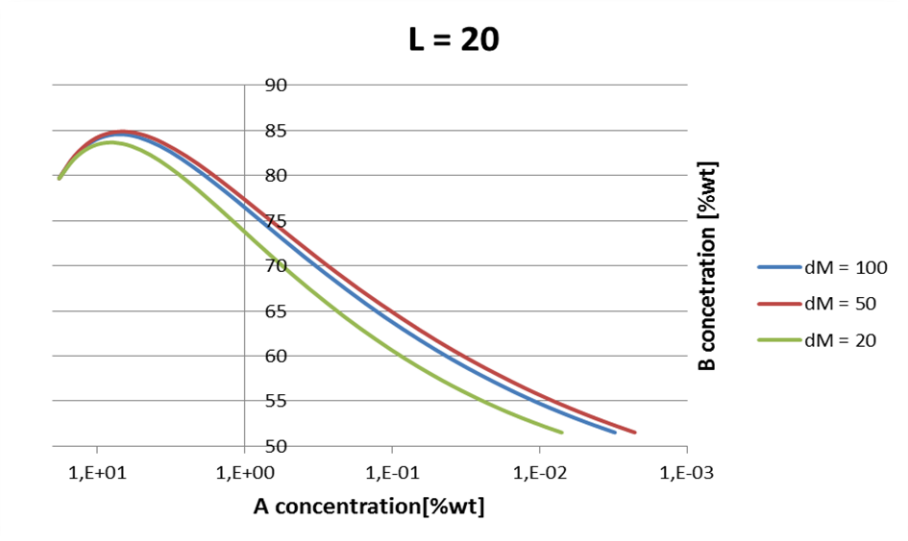

Figure 29: C_3 macro-pore size sensitivity for L = 20 micron; FEED 1

- **FEED 2:**

As seen for C_4 cut higher gain is obtained from the industrial feed, in the sensitivity on L we had 24.5% gain in B compared to the 18.6% of FEED 1 (for 0.01 %wt of A) resulted for L from 20 to 0.5 micron (figure 31). Concerning analysis on macro-pore size, L fixed at 5 micron is the only case (figure 32) in which B gain showed to be lower for than it was in FEED 1, in fact for dM from 100 to 20 micron gain is 6.9% (8.4% in FEED 1), while again no improvement is registered for smaller macro-pores. For L fixed at 20 micron we had again drop of selectivity for dM under 50 micron as in figure 33.

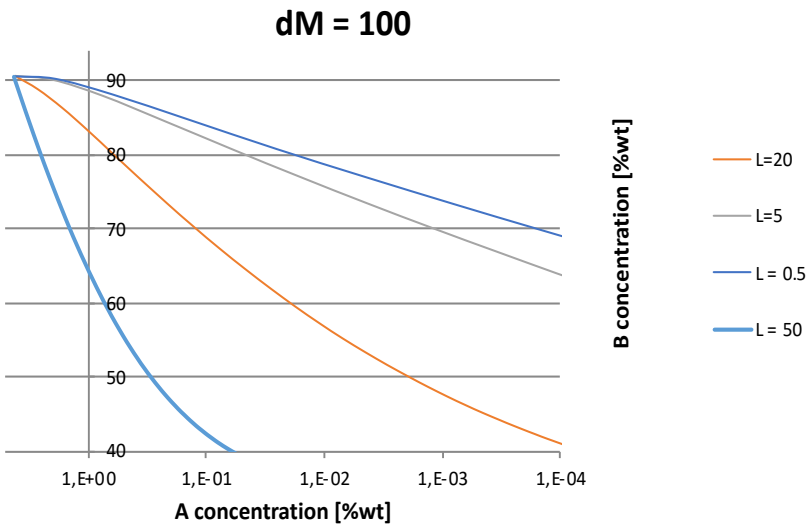

Figure 30: C_3 wall thickness sensitivity; FEED 2

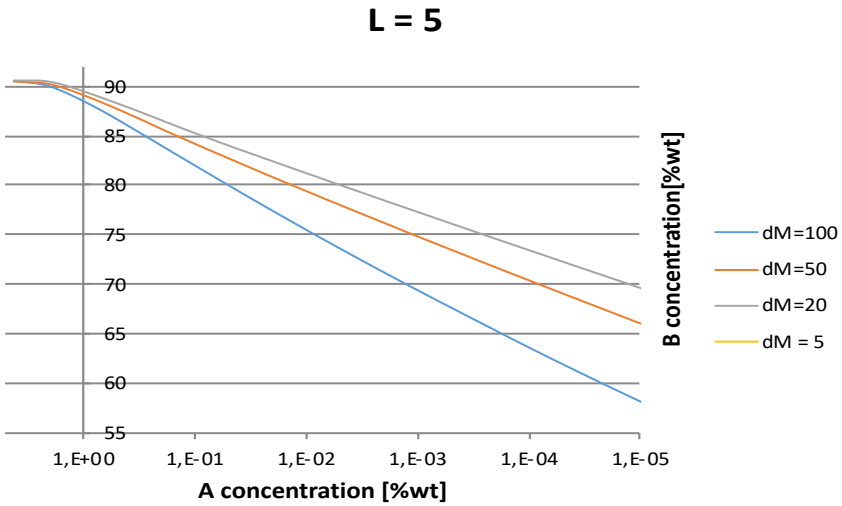

Figure 31: C_3 macro-pore size sensitivity for L = 5 micron; FEED 2

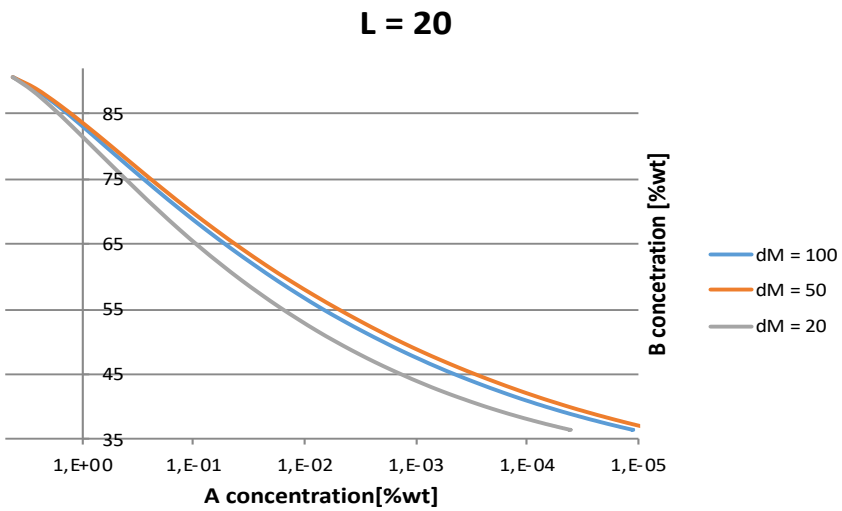

Figure 32: C_3 macro-pore size sensitivity for L = 20 micron; FEED 2

6.2.4 C_2 hydrogenation reactor profile

Ethylene cut showed lower sensitivity to textural parameters, in figure 34 profiles of L from 100 to 2 are displayed, for outlet A of 0.001%wt improvement in selectivity is just 0.44%, on the other hand A depletion resulted is pushed from 10.1 to 1.6 mass ppm for L from 100 to 2 micron.

It is clear that internal diffusion is here a much less limiting phenomenon, as well, moving toward low wall thickness L effect decreases even more.

As expected, simulation ran for fixed L of 2 micron (figure 35) showed minimal effect on both selectivity and impurity depletion, while for L of 50 micron (figure 36) neglectable improvement of selectivity, for 0.001%wt of A, and depletion is resulted for d_M of 400 to 200.

Under these values performance drop, if d_M of 20 is plugged, still with L of 50 micron, B in the outlet is 0.2% less (for A 0.001%wt) if compared to d_M of 200, with outlet A concentration from 1.6 to 5.6 mass ppm.
The results displayed in figure 34,35,36 also shows the effect of kinetic constants ratio on selectivity, in fact, while negative values selectivity was always calculated for C_4, C_3, ethylene is the only compound with positive values (table 9), in C_2 there is in fact no loss of product B, because loss is here balanced by its generation along the reactor.
This outcomes from kinetic constants ratio (k_1/k_2) which is around 22 for butene and propylene (Verdier, 2003) while 500 for ethylene (Bos *et al.*, 1993).

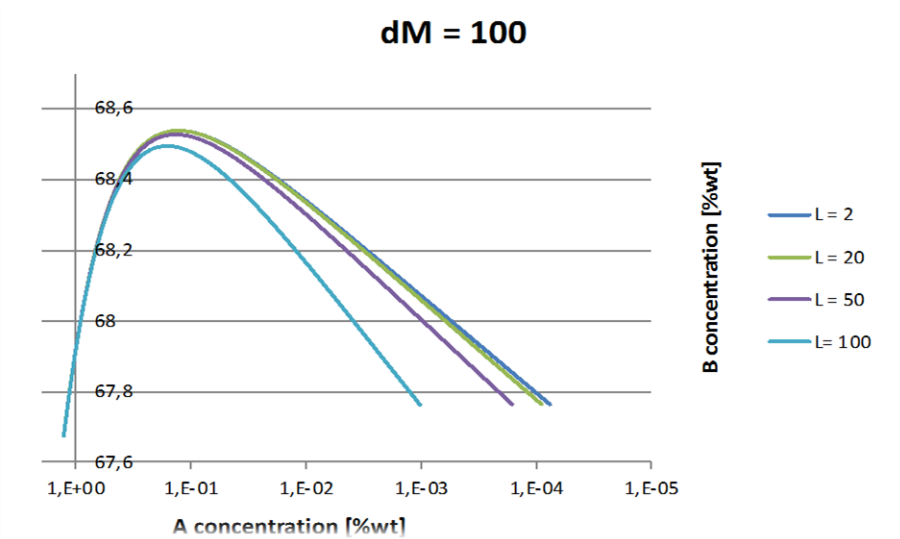

Figure 33: C_2 wall thickness sensitivity

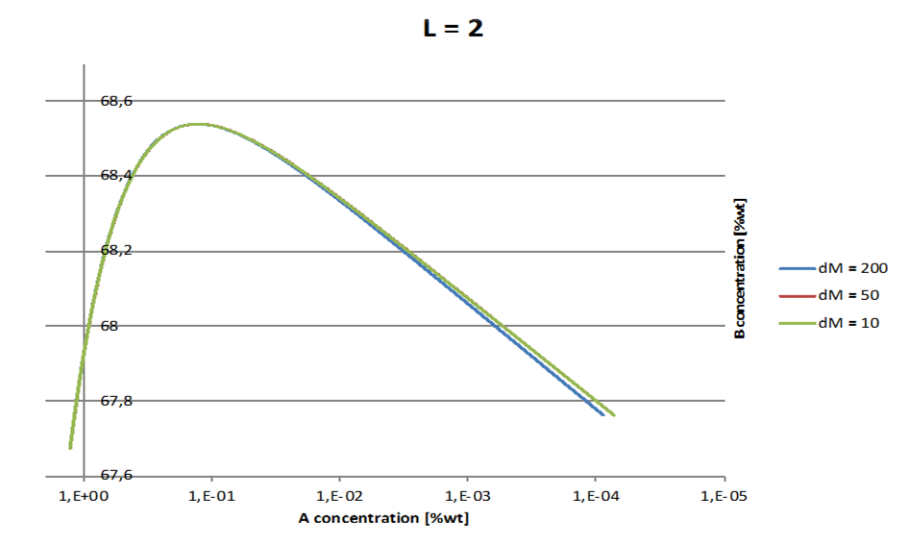

Figure 34: C_2 macro-pore size sensitivity for L = 2 micron

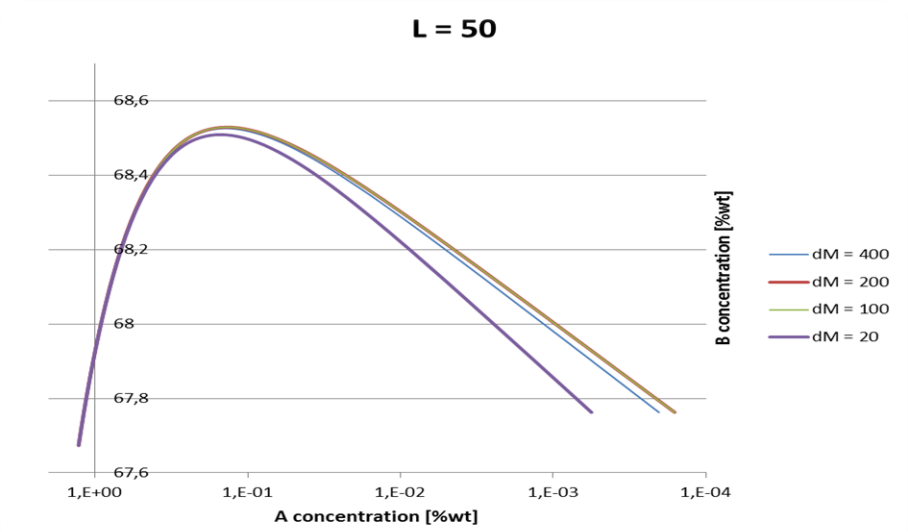

Figure 35: C_2 macro-pore size sensitivity for L = 50 micron

6.3 Comparisons

An attempt has been made to compare the performance of the monolith with a pellets fixed bed, for cut C_3 it has not been possible to obtain results in a pellets system due to the not convergence for wall thickness of 200 micron that is used to simulate pellets behavior, in fact an active phase coating of 0.2 mm (200 micron) is usually present on spherical pellets with diameter of 2-5 mm (Thomazeau and Boyer, 2011). High diffusion length can prevent the solution of the model, however we had convergence for cut C_4 and C_2, this because of the slower kinetics parameters. Moreover, just for C_2, pellets diameter has been plugged to 0.5 mm again to assure convergence, diameters above 2 mm resulted in lower specific area which prevented convergence of the algorithm in the internal loop (solution of balance (4)), these troubleshooting will be discussed in the net paragraphs. Data used for pellets fixed bed are reported in table 9.

Pellets fixed bed parameter	Value	Measure unit
Spherical particle diameter	2 (0.5 for C_2)	mm
Active phase coating thickness	0,2	mm
Reactor diameter	0,58	m
Flowrate	3,45E-03	$m^3 s^{-1}$
Superficial velocity	0,01	$m\ s^{-1}$
	H_2 FEED RATIO PELLETS/MONOLITH	
FEED 1	5/3	
FEED 2	1/1	

Table 11: Spherical pellets fixed bed operative condition

Results for C_4 (figure 37,38) showed that fixing A depletion to 0.01%wt we have a gap in B concentration of 35% for FEED 1 between pellets and monolith with wall of 50 micron thickness, while the gap is 18.9% for FEED 2. Regarding FEED 1, slightly higher depletion of A is reached in the pellets compared to one of the two monoliths because feed of hydrogen has been incremented by 5/3 ratio to obtain depletion desired, in FEED 2 the comparison is instead at equal conditions.

Concerning C_2 (figure 39) it is known from the previous results that due to its gas phase lower sensitivity results from the wall thickness, in fact the comparison at 0.01%wt showed just a gap of 0.4% in B concentration.

In conclusion, comparisons showed that for the two-phase cut C_4, and similar behavior is expected for C_3, consistent gap in selectivity toward B is present assuring substantially higher concentration of B in the outlet for the monolithic configuration, while for gas-phase cuts as C_2 the higher diffusion coefficient prevent the lower diffusion length in the monolith to be as effective.

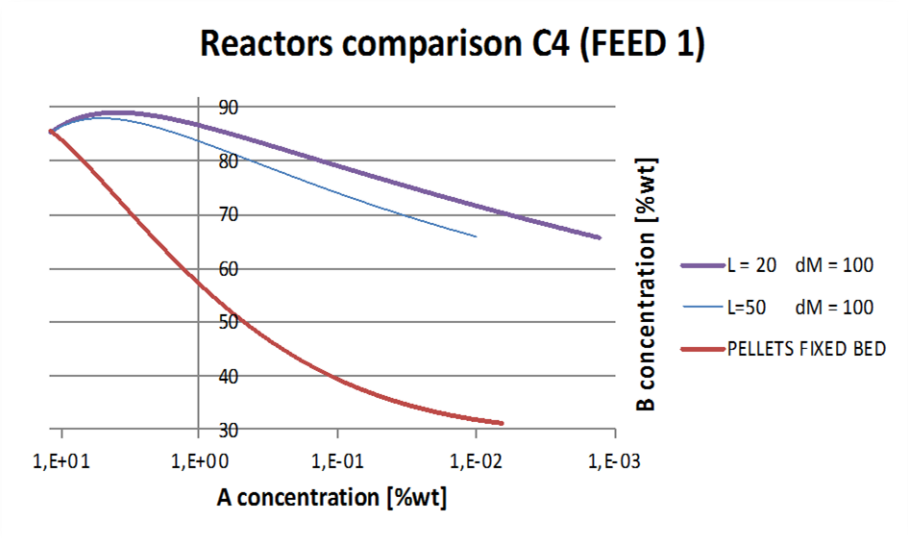

Figure 36: Profile of spherical pellets versus alveolar monolith for C_4; FEED 1

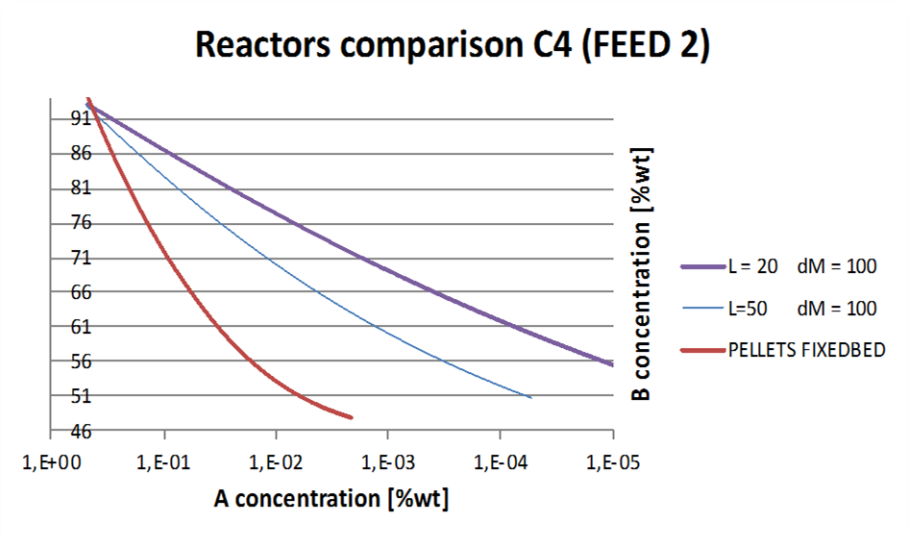

Figure 37: Profile of spherical pellets versus alveolar monolith for C_4; FEED 2

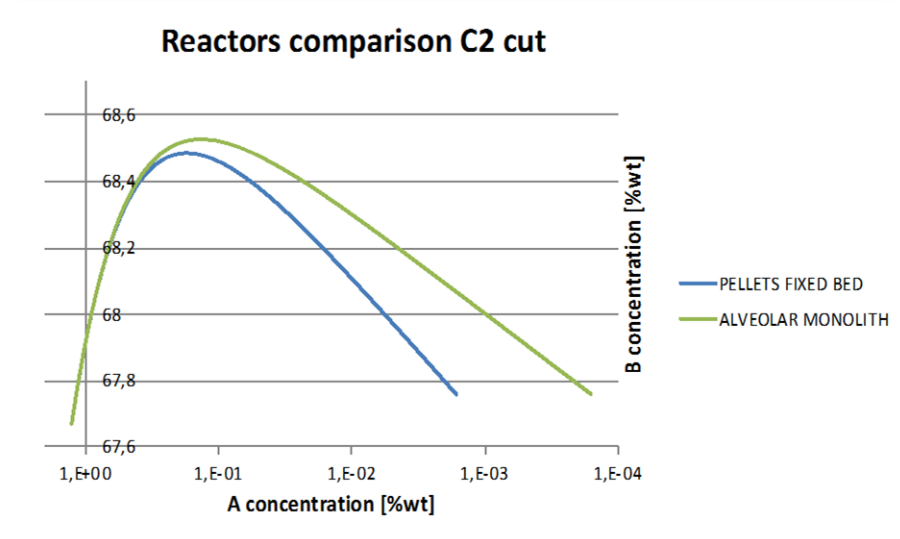

Figure 38: Profile of spherical pellets versus alveolar monolith for C_2

6.4 Pressure drops

Monoliths are typically characterized by low pressure drops if compared to pellets of different shapes, focusing on alveolar monoliths which are characterized by an open-cell structure, pressure drop magnitude will be strongly dependent on wall thickness and macro-pores diameter, where pressure drop is expected to rise for lower ratio d_M/L.

Low d_M/L ratio correspond to a structure with lower porosity (shells of small diameter with relatively thick walls), thus, while tuning d_M to lower values is usually associated with better selectivity and conversion it has also the counter effect of significantly rise pressure drop, overcoming drops in pellets fixed bed configuration.

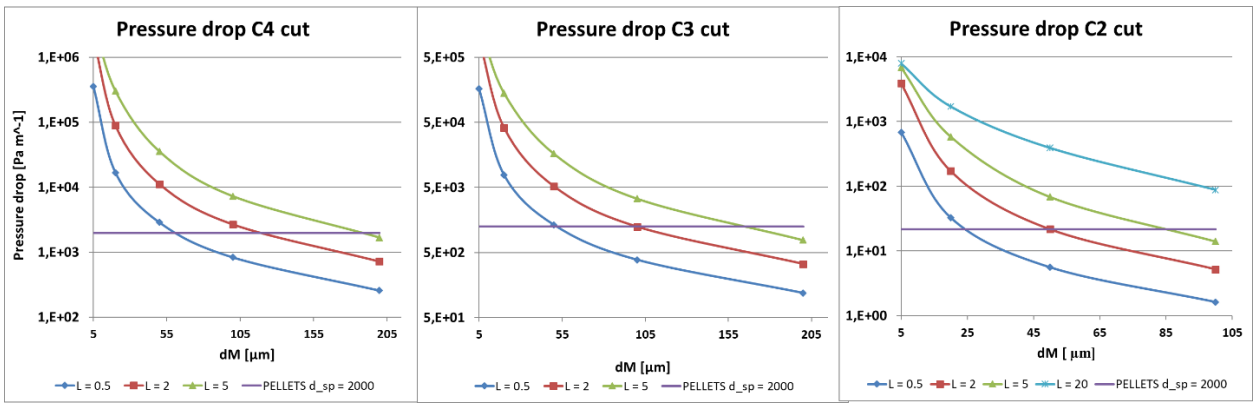

Figure 39: Pressure drop results as function of d_M for various L, comparison between monolith and pellets

Simulations results show strong dependence on d_M and L, if d_M tends to zero the correlations give us that pressure drop tends to infinite because void fraction of the monolith tends to zero.

On the ordinate axis, different range is shown for each cut, as expected we have lower drop for lighter cuts (figure 40).

- C_2 is only in gas-phase, therefore its pressure drop can be computed using Ergun equation, then alveolar monolith drop is computed with a literature correlation used for solid foams catalysts (Giani, Groppi and Tronconi, 2005), it comes out how the two configurations, pellets and monolith, have comparable pressure drop, monoliths give pressure one order of magnitude lower than spherical pellets for d_M of 100 micron with L of 2 micron, if d_M is tuned to 50 micron the same pressure drop is resulted, thicker L and lower d_M are associated with drops even higher than pellets. The area below pellets drop horizontal line is the optimal area for alveolar monoliths exploitment in term of pressure drop.
- C_3 is in mixed-phase, its pressure drop is expected to be higher for a number of factors. First, the presence of liquid gives higher average density to the fluid, second liquid phase is characterized by higher friction factor. Furthermore, co-existence of two phases gives ulterior friction phenomena between gas-liquid interphase which has to be taken into account, this is why more complex correlations, if compared to one-phase streams, need to be exploited in such cases (Bressa *et al.*, 2003; Giani, Groppi and Tronconi, 2005). It is so explainable a drop of one and a half order of magnitude from C_2 to C_3. Similarly to the lighter cut equivalent drop between pellets and monolith is here found for d_M of 100 micron and L of 2 micron, while for C_2 even point was found at d_M of 50 micron.
- C_4 is also in mixed-phase, almost half order of magnitude higher drop range is observed from C_3 to C_4. Equivalent drop between pellets and monolith is found for d_M slightly above 100 micron, for L of 2 micron.

Comparing monoliths optimal areas, looking at figure 40, C_2 could be considered as best compound for monolith exploitation, this because the range of texture that provide lower drop in the monolith gets more narrow moving to heavier cuts, however because the main objective is to ensure maximum selectivity, pressure drops can be seen as secondary as long as its proved to have lower or comparable drop than pellets configurations. Eventually, it is so been demonstrated that proper tuning of textural parameters is of main importance not only for selective hydrogenation performance, but also to assure a reasonable pressure drop that, depending on developers purpose, can be lower or equal to pellets system.

6.5 Summary

Putting together results from sensitivity analysis and results from pressure drop computation, we see that with the latter the selection of optimal monolith to exploit can be narrowed to the ones which showed pressure drop lower than spherical pellets system. This way the fraction of optimal configurations is severely reduced to the few green areas on figure 41,42. It can be noticed that values have been computed for two levels of depletion of A, as already seen in the previous paragraphs. Optimal texture proved to be for d_M of 100 micron and L under 2 micron (5 micron for C_2 cut), however correlation for monolith pressure drop could be too stringent and return too low values, otherwise green area could be extended to thicker walls which still assure performance superior to pellets technology.

Selectivity FEED 1						
		C4		C3 (*P = 25 bar)		C2
L	dM	1,E-02 %wt	1,E-03 %wt	1,E-02 %wt	1,E-03 %wt	1,E-03 %wt
100	100					0,15
50	100	-1,5				
20	100	-1,1	-1,5	-1,2		
5	100	-0,92	-1,4	-0,49	-0,83	
2	100	-0,92	-1,4			0,37
0,5	100			-0,27	-0,59	
5	300	-1,2				
5	100			-0,83		
5	50	-0,91	-1,4	-0,59		
5	20	-0,90	-1,4	-0,39		
20	300	-1,2				
20	200					0,34 (*L=50)
20	100	-1,1		-1,23		
20	50			-1,16		
20	20			-1,35		0,25(*L=50)
20	5	-1,4				

Figure 40: Selectivity results for FEED 1

Selectivity FEED 2					
		C4		C3 (*P = 25 bar)	
L	dM	0.01 %wt	0.001 %wt	0.01 %wt	0.001 %wt
100	100	-76			
50	100	-45			
20	100	-31	-47	-7,3	
5	100	-28	-42	-2,9	-4,4
2	100	-28	-42		
0,5	100			-2,1	-3,7
5	300	-31	-47		
5	100				-4,4
5	50	-28	-42		-2,9
5	20				-2,9
20	300	-35	-51		
20	200				
20	100	-31	-47		-10,1
20	50				-9,5
20	20				-9,2
20	5	-42	-60		

Figure 41: Selectivity results for FEED 2

6.6 Troubleshooting

The mathematical model coded on MATLAB presented a series of computation boundaries, convergence of the model is mainly limited by two parameters, wall thickness (2L) and kinetic constants (k_1/k_2).

L above 50 micron usually lead to non-convergence, due to failure in BVP solution or to non-convergence of tolerance toward desired value in the internal loop.

Kinetic constants of order of magnitude above $n \times 10^1 (kmol\ kg_{cat}^{-1} s^{-1})$ lead to failure in BVP solution even for smaller L, while for that same order of magnitude, only with C_3 kinetics, BVP solution failed for L above 50 micron.

- $C_4 : (k_1; k_2) = (1.574\,; 0.0676)$

While for L of 100 micron convergence is met, hence calculation algorithm returns solutions. However, for L of 200 micron convergence is not met in the internal computation loop due to error vector computation, the latter is coded as in equation 6.2, its computation doesn't meet tolerance generating a close loop in the computation algorithm (figure 17)

$$err(i) = \frac{|C_{is,new} - C_{is}|}{C_{is}} \quad \textbf{(6.2)}$$

$$i = A, B, C, H_2$$

Scalar values of vector $err(i)$ are updated with equation 4.7 as showed in figure 17. Surface concentration updating starts failing for compound A, this happens because A is the compound with the lowest concentration which is at the same time subject to depletion, for this reason (low concentration and negative reaction rate) equation 4.7, particularly for high values of L, is likely to return a negative or null second guess for the new computed surface concentration of A which makes updating diverge from the solution.
Attempt to obtain error convergence toward zero was made by imposing the new approximation for the surface concentration in case of a negative or zero value from equation 4.7, imposed value was a fraction of the bulk liquid concentration, the condition proved to be inefficient, error for compound A assumes periodic values.
Tolerance can be anyway met if a transfer parameters (namely mass transfer coefficient and surface area) are set to values lower enough to ensure that equation 4.7 updating won't produce a negative value preventing convergence.
Regarding pellets fixed bed, convergence is met until L of 200 micron (for both feed tested), this is obtained because of solid specific area that for this value of L is very low in the monolithic configuration, for pellets fixed bed convergence is met for spheres diameter up to 2000 micron (2 mm)

- $C_3 : (k_1; k_2) = (13.83 ; 0.629)$

For both L of 200 and 100 convergence is not met, this time error is inside BVP solver tool *bvp5c*. MATLAB tool consists in a pre-coded computation routine programmed to solve DAE systems using a collocation method, in these cases a singular matrix is encountered, for this reason the matrix cannot be inverted as it is necessary to reach system solution. The reason for the absence of convergence for L of 100 micron is due to the faster kinetics.
Only C_3 presented ulterior cases of not convergence of the model, during sensitivity simulations on d_M for L of 20 micron, solution was not reached for extreme values of diameter, namely for 5 and 300 micron, for both feed composition attempted, bug was found in the internal loop values of error vector regarding compound A, therefore imputable to specific area and facilitated by the faster kinetics of the cut.
During the same sensitivity analysis but for L of 5 micron convergence was instead met for d_M of 5 micron because of the higher surface area due to d_M/L ratio.
Even considering pellets catalyst, singular matrix has been encountered in the BVP for L of 200 and 100 micron. Singular matrix was also encountered with different composition.
Because the same diffusivity is plugged for C_3 and C_4, and small difference in liquid density, phase distribution and starting concentrations is present, thus it is higher kinetic constants that prevent solution from convergence inside the BVP solver.

- $C_2 : (k_1; k_2) = (1.64 ; 0.0033)$

For L of 100 micron system solution is reached, if instead L = 200 micron is plugged, then no singular matrix is encountered in the BVP but convergence is not met for compound A which enters in a loop of error values, the problem is due to the low surface area which, due to equation 4.7, returns a negative value for the updated surface concentration. As for the other cuts the computation problem is not resolved by imposing a new approximation, however in the case of pellets fixed bed, the higher value of surface area enables convergence of tolerance until the last reactor infinitesimal volume, a comparison with monolith has thus been possible. Convergence was still limited to pellets diameter not over 500 micron (0.5 mm).

7 Conclusions

Selective hydrogenation is a process that requires strict purification performances, these have to be obtained in the most cost and energy effective way possible, conventional packed-bed reactors are subject to physico-chemical drawbacks consisting in limited mass transfer, low contact area and internal diffusion limitations.
Because conversion specifications impose a total depletion of the polyunsaturated compounds, reactive system has to be designed in order to guarantee required performance with minimum amount of material expenses, particularly in terms of Palladium active phase, especially in terms of selectivity to minimize further hydrogenation from olefin, product of interest, to the saturated specie.
Consequently, hierarchically organized porous monolithic materials, has been sensitively analyzed to probe and optimize their macro-scale textural parameters looking forward a future built of a selective hydrogenation pilot unit adopting alveolar monolith catalyst support.
In the work, it has been shown the texture flexibility from the synthesis of these monolithic supports, these can be produced in a wide range of dimensions of the void shells and shell's wall thickness.
It has been demonstrated that selectivity and particularly reactant depletion are sensibly dependent on the aforementioned features. Results showed a need for smaller skeleton thickness, large gain in depletion and selectivity is obtained in C_3 cut, due to its fast kinetics, for thickness plugged from 50 micron down to 0.5, C_4 instead, for the operative condition tested, displayed less sensibility for wall thinner than 5 micron, while noticeable gain in performances was visible from 50 micron to 5.
Tests on C_2 cut, being characterized by higher diffusion coefficients, manifested the lowest sensibility on meso-pore length hence lowest internal diffusion limitation, impurity depletion revealed here the best performances among the tested cuts due to the fact that much higher kinetic constants ratio (Bos *et al.*, 1993) was present in C_2 compared to C_3 and C_4.
A further series of simulation analyzed the effect of macro-pores diameter on selectivity, in this case smaller diameters showed two competitive effects, mass transfer coefficient rise and surface area drop, for such reason pore volume cannot fall under a threshold that depends on d_M/L ratio, namely, a low wall thickness moves the threshold toward lower macro-pore volume ensuring wider range of positive effect for d_M decreasing.
C_4 cut showed selectivity loss for d_M under 50 micron with L of 5 and under d_M of 100 with L of 20, C_3 lost selectivity under 20 micron with L of 5 and under 50 with L of 20, finally C_2 showed neglectable sensitivity.
Moreover, ulterior design aspect of pressure drop has been taken into account proving that thin walls and big macro-pores reduces pressure drop, calculation displayed that a diameter above 100 micron for C_4, C_3 while above 50 for C_2 is needed to have resulting pressure drop lower than for spherical pellets.
Exploiting the model, optimal area of textural properties has been found for various cuts, exploiting the major advantage that alveolar monolith can be synthetized adapting them to different reaction systems and operating conditions.
In perspective, plenty of work can still be done to improve the coded model, comparisons with commonly adopted technologies where limited by numerical resolution of the BVP for thick internal diffusion layers.

As well, a sensitivity on H_2 feed and a study on systems with multiple injections of hydrogen could lead to further optimization in feed distribution.

Next model development could include energy balances for not isothermal systems, in order to analyze systems which are closer to industrial practice where hydrogenation is mostly operated adiabatically (Mohundro, 2003).

Sensitivity analysis should be also foreseen to probe variation of more parameters at a time (L,d_M) adopting design on experiments methods.

List of symbols

C_2	Hydrocarbons with two carbon atoms
C_3	Hydrocarbons with three carbon atoms
C_4	Hydrocarbons with four carbon atoms
H_2	Hydrogen
CO	Carbon monoxide
MTBE	Methyl tert-butyl ether
$\varepsilon, \varepsilon_B$	Bulk porosity (-)
ε_{Bm}	Bulk porosity of the monolith (-)
ε_w	Wall porosity of the monolith (-)
τ	Tortuosity (-)
T	Temperature (°C or K)
P	Pressure (bar)
R	Gas constant 8,314 (J mol^{-1} K^{-1})
ΔT	Temperature difference (°C)
ΔP	Pressure drop (Pa)
2L	Shell-wall thickness (µm)
d_M	Egg-shell diameter (µm)
G/L	Gas-Liquid
A	Poly-unsaturated hydrocarbon
B	Mono-unsaturated hydrocarbon
C	Saturated hydrocarbon
r_i	Reaction rate for reaction number 'i' (mol kg^{-1} s^{-1})
k_i	Kinetic constant of reaction number 'i' (mol kg^{-1} s^{-1})
K_i	Adsorption constant of compound 'i' (-)
x_i	Molar fraction of compound 'i' (-)
C	Molar concentration (mol m^{-3})
C_{iS}	Concentration of compound 'i' on shell-wall surface (mol m^{-3})
D_{iL}	Diffusivity of compound 'i' in the liquid phase (m^2 s^{-1})
D_{iG}	Diffusivity of compound 'i' in the gas phase (m^2 s^{-1})
$D_{e,i}$	Effective diffusivity of compound 'i' defined as: $D_i(\varepsilon/\tau)$ (m^2 s^{-1})
ρ_w	Mass density of catalyst (kg m^{-3})
ρ_L	Mass density of the liquid phase (kg m^{-3})
ρ_V	Mass density of the gas phase (kg m^{-3})
y	Shell-wall depth coordinate
z	Reactor length coordinate
Z	Reactor length (m)
dz	Infinitesimal reactor length (m)
$\dot{V}_L$	Liquid flowrate (m^3 s^{-1})
$\dot{V}_G$	Gas flowrate (m^3 s^{-1})
$\dot{n}_G$	Molar flowrate of the gas phase (mol s^{-1})
C_{iG}	Concentration of compound 'i' in the gas phase (mol m^{-3})
C_{iL}	Concentration of compound 'i' in the liquid phase (mol m^{-3})
J_i^{GL}	Molar flow of compound 'i' at gas-liquid interphase (mol s^{-1} m^{-2})
J_i^{LS}	Molar flow of compound 'i' at liquid-solid interphase (mol s^{-1} m^{-2})
k_{iGf}	Mass transfer coefficient of compound 'i' at the interphase gas-liquid in the gas film (m s^{-1})
k_{iLf}	Mass transfer coefficient of compound 'i' at the interphase gas-liquid in the liquid film (m s^{-1})
k_{iL}	Mass transfer coefficient of compound 'i' at the interphase gas-liquid, calculated as the average: $k_{iL} = [(k_{iGf}{}^{-1})(k_{iLf}{}^{-1})]^{-1}$ (m s^{-1})

k_{iL}	Mass transfer coefficient of compound 'i' at the interphase gas-liquid (m s^{-1})
k_{iS}	Mass transfer coefficient of compound 'i' at the interphase liquid-solid (m s^{-1})
H_i	Henry's law constant (-)
η	Effectiveness factor, defined as ratio of reaction rate at shell-wall surface and average reaction rate in shell-wall
a_L	Specific area of gas-liquid interphase (m^2 m^{-3})
a_S	Specific area of liquid-solid interphase, assumed equal to catalyst specific area (m^2 m^{-3})
r_{iS}	Reaction rate at catalyst surface (mol s^{-1} m^{-3})
S	Catalyst available surface (m^2)
u_L	Flow speed of the liquid phase (m s^{-1})
u_V	Flow speed of the gas phase (m s^{-1})
u_i	Flow speed of phase 'i' (m s^{-1})
μ_L	Dynamic viscosity of the liquid phase (Pa s)
Re	Reynolds number defined as: ($u\rho d/\mu$) (-)
Sc	Schmidt number defined as: ($\mu/\rho d$) (-)
Sc_{iL}	Schmidt number of compound 'i' in the liquid phase (-)
d_{conn}	Diameter of inter-connecting pores between shells, fixed as $d_M/10$ (μm)
N_{conn}	Number of inter-connections per shell, fixed at 2 (-)
d_{sp}	Diameter of spherical pellets (m)
ε_L	Liquid hold-up defined as: $(\varepsilon - 0.28)\ uV\ /\ (uL + uV)$ (-)
d_h	Equivalent particle diameter defined as: $(\varepsilon_L\ d_{ps} / [\ 1.5(1 - \varepsilon_L)])$ (m)
σ	Surface tension (N m^{-1})
g	Gravitational acceleration: 9.81 (m s^{-2})
ξ_{VL}	Coefficient defined as: $\varepsilon^{-1}[(u_L u_V)\Delta P + (u_L\rho_L + u_V\rho_V)]g$
f_P	Friction factor for one-phase flow in spherical pellets
f_M	Friction factor for one-phase flow in alveolar monolith
f_{GL}	Friction factor for two-phase flow (C_3, C_4)
S_B	Selectivity in the mono-unsaturated compound B (-)
W_{A1}	Mass fraction of compound A in reactor's inlet (%wt)
W_{B1}	Mass fraction of compound B in reactor's inlet (%wt)
W_{C1}	Mass fraction of compound C in reactor's inlet (%wt)
W_{A2}	Mass fraction of compound A in reactor's outlet (%wt)
W_{B2}	Mass fraction of compound B in reactor's outlet (%wt)
W_{C2}	Mass fraction of compound C in reactor's outlet (%wt)

List of figures

Figure 1: MEB pictures of Si(HIPE) monolith porosity, extreme cases for macro-pores dimension (figure from (Destribats et al., 2012)) 2
Figure 2: Pictures of monoliths (right), MEB pictures of alveolar monoliths and representation of the wall 2
Figure 3: Scheme of crude oil fractioning and first processing steps (upstream refining) 4
Figure 4: Scheme of downstream treatment of cracker effluents (figure from ("Hydrogenation Reactions" in: Handbook of Heterogeneous Catalysis', 2008)) 5
Figure 5: Scheme of olefins value chain 7
Figure 6: scheme of a selective hydrogenation process for C_3 cut, configuration with two adiabatic reactors (multi-stage) with intercooling and a separation step (figure from (Thomazeau and Boyer, 2011) with modifications) 9
Figure 7: upflow and downflow scheme for fixed bed hydrogenation reactor 10
Figure 8: Porosity of Si(PHIPE) alveolar monoliths (left), example of meso-pore size distribution for alveolar monolith $_{2.6}Si(PHIPE)_{85H}$ (right) (from (Destribats et al., 2012)) 12
Figure 9: simplified texture of an alveolar monolith synthetized as polyHIPE 13
Figure 10: Scheme of plug flow reactor model 14
Figure 11: Scheme of complete wetting(left) and partial wetting(right) for the interfaces in a three-phase system 15
Figure 12: Reaction scheme for hydrogenation of polyunsaturated compounds 16
Figure 13: Graphic representation of molar fraction profile inside the wall 18
Figure 14: Three-phase reactor graphic representation, overall reactor (left), infinitesimal volume (right) 19
Figure 15: Interphase mass transfer representation 20
Figure 16: Schematic representation of the calculation algorithm coded on MATLAB 23
Figure 17: A and B molar fraction wall profile in C_4 for different wall thickness (2L), wall surface is for y/L = 1 28
Figure 18: B molar fraction wall profile for C_4, wall surface is for y/L = 1 29
Figure 19: A and B molar fraction wall profile for C_3 30
Figure 20: A and B molar fraction wall profile for C_2 31
Figure 21: C_4 wall thickness sensitivity FEED 1 34
Figure 22: C_4 macro-pore size sensitivity for L = 5 micron ; FEED 1 35
Figure 23: C_4 macro-pore size sensitivity for L = 20 micron ; FEED 1 35
Figure 24: C_4 wall thickness sensitivity; FEED 2 36
Figure 25: C_4 macro-pore size sensitivity for L = 5 micron; FEED 2 36
Figure 26: C_4 macro-pore size sensitivity for L = 20 micron; FEED 2 37
Figure 27: C_3 wall thickness sensitivity; FEED 1 37
Figure 28: C_3 macro-pore size sensitivity for L = 5 micron ; FEED 1 38
Figure 29: C_3 macro-pore size sensitivity for L = 20 micron ; FEED 1 39
Figure 30: C_3 wall thickness sensitivity; FEED 2 39
Figure 31: C_3 macro-pore size sensitivity for L = 5 micron; FEED 2 40
Figure 32: C_3 macro-pore size sensitivity for L = 20 micron; FEED 2 40
Figure 33: C_2 wall thickness sensitivity 41
Figure 34: C_2 macro-pore size sensitivity for L = 2 micron 41
Figure 35: C_2 macro-pore size sensitivity for L = 50 micron 42
Figure 36: Profile of spherical pellets versus alveolar monolith for C_4 ; FEED 1 44
Figure 37: Profile of spherical pellets versus alveolar monolith for C_4 ; FEED 2 44
Figure 38: Profile of spherical pellets versus alveolar monolith for C_2 45
Figure 39: Pressure drop results as function of d_M for various L, comparison between monolith and pellets 45
Figure 40: Selectivity results for FEED 1 47
Figure 41: Selectivity results for FEED 2 48

List of tables

Table 1: Selective hydrogenation specifications for production of intermediaries for petrochemistry *6*
*Table 2: Molar fractions of C2 to C4 cuts after cracking and separation steps; A polyunsaturated compound, B monounsaturated compound, C: saturated compound. *cut C4 composition after extraction of 1,3-butadiene.* *6*
Table 3: Porosity and tortuosity factors for diffusion in catalysts *8*
Table 4: Activity and selectivity of metallic active phases for hydrogenation reactions *8*
Table 5: Supports coupled with active phase *8*
Table 6: Choice of reactors for selective hydrogenation *10*
Table 7: BVP problem variables and parameters, C3 cut processed with higher pressure to have a bi-phasic flow *27*
Table 8: Composition of inlet feeds simulated *33*
Table 9: spherical pellets fixed bed operative condition *43*

List of equations

Equation 4.1 ..... *17*
Equation 4.2 ..... *17*
Equation 4.3 ..... *18*
Equation 4.4 ..... *20*
Equation 4.5 ..... *20*
Equation 4.6 ..... *20*
Equation 4.7 ..... *35*
Equation 4.8 ..... *22*
Equation 4.9 ..... *22*
Equation 4.10 ..... *22*
Equation 6.1 ..... *32*
Equation 6.2 ..... *49*

Reference list

Alves, J.A. *et al.* (2012) 'Kinetic study of the selective catalytic hydrogenation of 1,3-butadiene in a mixture of n-butenes', *Journal of Industrial and Engineering Chemistry*, 18(4), pp. 1353–1365. doi: 10.1016/j.jiec.2012.01.038

Arnold, H., Dobert, F. and Gaube, J. 'Handbook of Heterogeneous Catalysis', 14.10.1.

Bos, A.N.R. *et al.* (1993) 'A kinetic study of the hydrogenation of ethyne and ethene on a commercial Pd/Al2O3 catalyst', *Chemical Engineering and Processing: Process Intensification*, 32(1), pp. 53–63. doi: 10.1016/0255-2701(93)87006-G

Bressa, S.P. *et al.* (2003) 'Analysis of operating variables on the performance of a reactor for total hydrogenation of olefins in a C3,C4 stream', *Chemical Engineering Journal*, 92(1-3), pp. 41–54. doi: 10.1016/S1385-8947(02)00116-X

Destribats, M. *et al.* (2012) 'Tailored Silica Macrocellular Foams: Combining Limited Coalescence-Based Pickering Emulsion and Sol-Gel Process', *Advanced Functional Materials*, 22(12), pp. 2642–2654. doi: 10.1002/adfm.201102564

Feinle, A., Elsaesser, M.S. and Hüsing, N. (2016) 'Sol-gel synthesis of monolithic materials with hierarchical porosity', *Chemical Society Reviews*, 45(12), pp. 3377–3399. doi: 10.1039/c5cs00710k

Giani, L., Groppi, G. and Tronconi, E. (2005) 'Mass-Transfer Characterization of Metallic Foams as Supports for Structured Catalysts', *Industrial & Engineering Chemistry Research*, 44(14), pp. 4993–5002. doi: 10.1021/ie0490886

Heck, R.M., Gulati, S. and Farrauto, R.J. (2001) 'The application of monoliths for gas phase catalytic reactions', *Chemical Engineering Journal*, 82(1-3), pp. 149–156. doi: 10.1016/S1385-8947(00)00365-X

'"Hydrogenation Reactions" in: Handbook of Heterogeneous Catalysis' (2008).

Mohundro, E.L. (2003) 'Overview on C2 and C3 Selective Hydrogenation in Ethylene Plants'.

Octave Levenspiel (1999) *Chemical Reaction Engineering*. 3rd edn. United States of America: John Wiley & Sons.

Samimi, F. *et al.* (2014) 'DE Approach in Development of a Detailed Reaction Network for Liquid Phase Selective Hydrogenation of Methylacetylene and Propadiene in a Trickle Bed Reactor', *Industrial & Engineering Chemistry Research*, 54(1), pp. 117–129. doi: 10.1021/ie503600b

Silverstein, M.S. (2014) 'Emulsion-templated porous polymers: A retrospective perspective', *Polymer*, 55(1), pp. 304–320. doi: 10.1016/j.polymer.2013.08.068

Thomazeau, C. and Boyer, C. (2011) 'Hydrogénation des hydrocarbures'.

Verdier, S. (2003) 'Pd–Sn/Al2O3 catalysts from colloidal oxide synthesis II. Surface characterization and catalytic properties for buta-1,3-diene selective hydrogenation', *Journal of Catalysis*, 218(2), pp. 288–295. doi: 10.1016/S0021-9517(03)00064-2

8 Acknowledgements

This thesis work has been carried out from March to July 2018 at the research center *IFP Energies Nouvelles* of Solaize, France, in the Department of *kinetic modellization*.
I owe my sincere gratitude to my supervisors, for their availability, theoretical support, kindness and insight.
The previous sentence refers to Verstraete Jan, Ph.D, for support regarding kinetic modelling, as well as to Uzio Denis Ph.D, for support regarding selective hydrogenation catalysis.
I owe peculiar gratitude to Mekki-Berrada Adrien Ph.D, for being always available for advise and support during the internship, even anticipating future questions and upcoming issues.
Moreover, I have to express my gratitude for the environment found in the workplace, especially for the many interns who shared this experience with me and providing ideas, suggestions and friendship. A felt recognition goes to my colleague Brian, for the precious help in coding the script and to my brother Simone for having been always available not only during the thesis work but throughout my university studies.
In conclusion, I thank my tutor in *Politecnico di Torino*, Specchia Stefania Ph.D, for the availability during the thesis work and for the mediation which was fundamental to discover and carry out this thesis opportunity.